Elisabeth Anna Schöffmann, BSc

Evaluation of microfluidic systems for the cultivation of algae

MASTERARBEIT

zur Erlangung des akademischen Grades

Master of Science

Masterstudium Chemie

eingereicht an der

Technischen Universität Graz

Betreuer

Assoc.Prof. Dipl.-Chem. Dr.rer.nat. Torsten Mayr

Institute of Analytical Chemistry and Food Chemistry
Graz University of Technology

Graz, Dezember 2017

EIDESSTATTLICHE ERKLÄRUNG

Ich erkläre an Eides statt, dass ich die vorliegende Arbeit selbstständig verfasst, andere als die angegebenen Quellen/Hilfsmittel nicht benutzt, und die den benutzten Quellen wörtlich und inhaltlich entnommenen Stellen als solche kenntlich gemacht habe. Das in TUGRAZonline hochgeladene Textdokument ist mit der vorliegenden Masterarbeit identisch.

Datum

Unterschrift

Widmung

Ich widme diese Arbeit meiner gesamten Familie, die mich immer und überall unterstützt.

Zusammenfassung

Das Hauptziel dieser Arbeit war es, ein Grundverständnis im Umgang mit Algen und mikrofluidischen Systemen und der Korrelation zwischen Algenzahl und Fluoreszenz beziehungsweise mit dem Absinken der Sauerstoffkonzentration in der Dunkelphase zu erhalten.

Im Detail enthält dies die Kultivierung der Batch-Kulturen, die Herstellung der Nährlösungen für die Algen, den Umgang mit den mikrofluidischen Chips, die Integration von Sauerstoffsensoren in die Kammern, als auch das Messen mit optischen Messgeräten.

Optische Sensoren haben ein breites Anwendungsspektrum und sind leicht miniaturisierbar. Daher ist die Verwendung von mikrofluidischen Chips eine gute Versuchsgrundlage für die Untersuchung der Algenrespiration.

Für die Untersuchung von unterschiedlichem Respirationsverhalten wurden drei Algenarten ausgewählt, chlorella vulgaris, phaedactylum tricornutum und pleurochrysis elongata.

Die besten Versuchsbedingungen wurden mit chlorella vulgaris, einer Grünalgenart, aufgrund ihrer Größe und geringen Mobilität erhalten. Ein Respirationsschnelltest wurde erfolgreich entwickelt.

Abstract

The aim of this work was to get an understanding of working with algae and microfluidic chips and to correlate algae cell number with fluorescence and the fall of oxygen concentration in the darkness.

In detail this includes cultivating of batch cultures, mixing of algae nutrition media, closing and filling of microfluidic chips, integration of oxygen sensor spots into the chambers and measuring with optical devices.

Optical sensors have a broad spectrum of applications and are easy to miniaturise. Therefore appropriation with microfluidic chips for the study of respiration of algae is a good trial content.

Three algae types were chosen to observe different behaviours in respiration, chlorella vulgaris, phaedactylum tricornutum and pleurochrysis elongata. Best test procedure was obtained with chlorella vulgaris, a type of green algae, because of their size and low mobility. A rapid respiration assay was successfully implemented.

Table of Content

1. Introduction

Algae have a good observable respiration metabolism, where oxygen is produced in the presence of light and oxygen is consumed in the dark. Their growth is fast and they have a rapid response on changes in their environment. For monitoring and recording optical sensors have a broad range of applications, they are fast responding and good integrate-able in small areas. Their basic principle is the conversion of light beams into electric signals in which they work in a non-destructive way.

The combination of optical sensors with microfluidic systems, which advantages of small volumes and the possibility to integrate many different functionalities, marks a miniaturized and fast way for the study of living organisms, like algae.

The aim of this thesis was to observe if growing algae in microfluidic chips and their monitoring with optical oxygen sensors is possible to implement.

Therefore a combination of algal respiration measurement with optical oxygen sensors and automatic counting of cell numbers on the microscope were a goal to examine.

2. Theoretical Background

2.1. Principles of luminescence

Most parts of this section were taken from [5] and [3].

Introduction

Luminescence is defined as the emission of visible ultraviolet photons by a substance. Contrary to incandescence, luminescence does not dependent on a rise in temperature, i.e. it is not resulting from heat. Several types of luminescence are classified based on the mode of excitation. Some of them are listed in Table 1.

Table 1: Luminescence phenomena

Phenomenon	Excitation
Photoluminescence	Photons
Electroluminescence	Electric field
Chemiluminescence	Chemical process
Radioluminescence	Radiation
Bioluminescence	Biochemical process
Triboluminescence	Electrostatic forces

Fluorescence is a special case of luminescence and part of photoluminescence. The interaction of light with matter can result either into scattering or absorption. The latter is the origin of photoluminescence, as shown in Illustration 1.

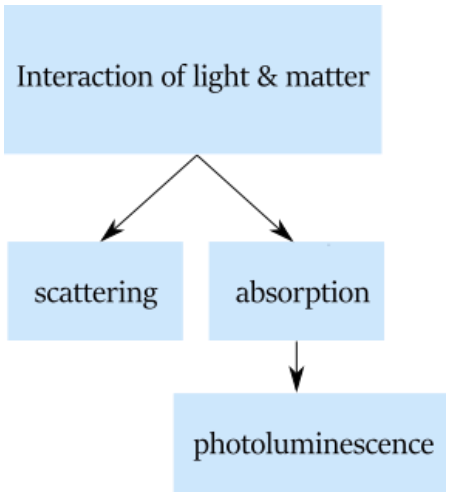

Illustration 1: Light-matter interaction and the result of photoluminescence due to absorption (emission) of light (photons). [3]

2.1.1. Absorption of visible UV light

2.1.1.1. Types of electronic transitions

Electronic transition always consists of the rise of an electron from the ground state to an unoccupied orbital due to the absorption of a photon. The molecule is then in the excited state. There are different molecular orbitals, which will be discussed shortly. The σ-orbital is either formed by two s-orbitals or from a combination of s- and p-orbitals. The resulting bond is then called an σ-bond. A so-called π-bond results from a π-orbital which is formed from two p-orbitals overlapping laterally. As an example, the π-bond of ethylene is shown in Illustration 2 for visualization purposes.

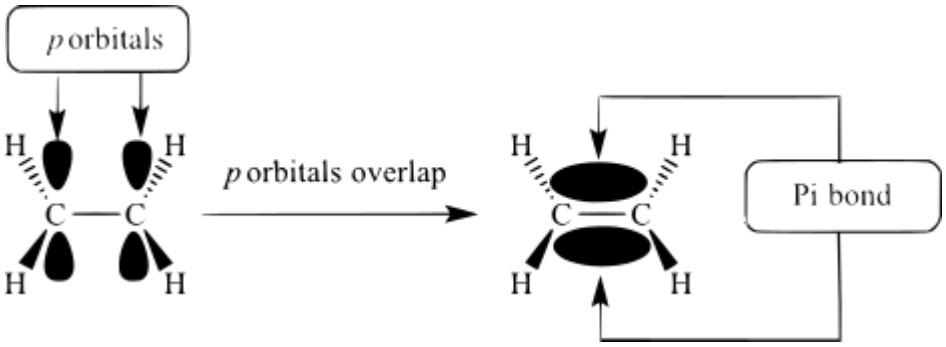

Illustration 2: Illustration of the π-bond of ethylene.

2.1.1.2. Beer-Lambert law

Assume light at a given wavelength λ is absorbed by an absorbing medium. The efficiency of absorption is characterized by the absorbance A(λ) or transmittance T(λ) defined as

$$A(\lambda) \stackrel{\text{def}}{=} \log_{10} \frac{I_\lambda^0}{I_\lambda} = -\log_{10} T(\lambda)$$

where the transmittance is given as the inverse ratio of the light intensities.

$$T(\lambda) = \frac{I_\lambda}{I_\lambda^0}$$

The light intensities are denoted by I_λ^0 for the beam entering the absorbing medium and I_λ for the beam leaving the absorbing medium. The Beer-Lambert-Law is then given by

$$A(\lambda) \stackrel{\text{def}}{=} \log_{10} \frac{I_\lambda^0}{I_\lambda} = \varepsilon(\lambda) l c$$

where $\varepsilon(\lambda)$ is the *molar absorption coefficient* (L mol^{-1} cm^{-1}), c is the concentration (mol L^{-1}) of the absorbing substance and *l* is the *absorption path length* (cm). The molar absorption coefficient is a quantity which describes the ability of a molecule to

absorb light in a solvent. By modelling the molecule as an oscillating dipole one can define the oscillator strength

$$f = \frac{4.32 \times 10^{-9}}{n} \int \varepsilon(k) dk$$

where k is the wavenumber (cm^{-1}) and *n* is the refraction index. The constant in the numerator can be calculated from the mass and charge of an electron and the speed of light.

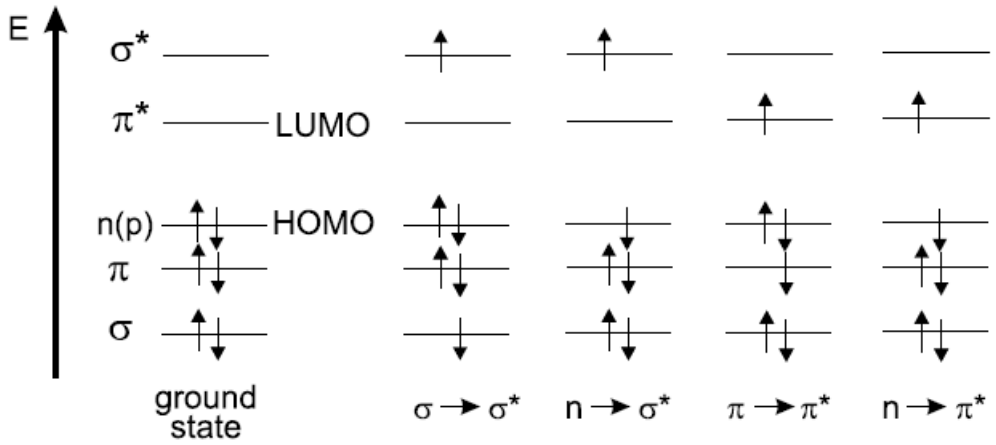

Illustration 3: Exemplary the energy levels of molecular orbitals in formaldehyde and possible electronic transitions. [3]

For $n \rightarrow \pi^*$ transitions, values of the molar absorption coefficient are in the order of 10^2 and the oscillator strength about 10^{-3}. For $\pi \rightarrow \pi^*$ transitions the oscillator strength reaches its maximum for some compounds. For the transition between initial and final states, one can introduce the concept of transition moments which is of major importance for experiments with polarized light. The transition moment can be understood as a vector in a coordinate system defined by the atom nuclei. Therefore, molecules whose transition moment is parallel to the electrical vector of linearly polarized light are excited more likely. By computing the dot product between the electrical vector and the transition moment, one can state that the excitation probability is proportional to the square of the dot product. From basic mathematics the dot product is zero only if two vectors are orthogonal and at its maximum only if two vectors are parallel. From these considerations one can show that the transition probability is zero if the electrical vector and the transition moment are orthogonal and largest if the two vectors are parallel.

2.1.1.3. Franck-Condon principle

The basis of the Franck-Condon principle is given by the observation that rise of an electron to an antibonding orbital takes about 10^{-15} seconds. Compared to the characteristic time of molecular vibrations, this is a very quick procedure. Thus, electronic transitions occur without changes in the nuclei positions. The resulting state is then called a Franck-Condon state and the transition is known as vertical transition.

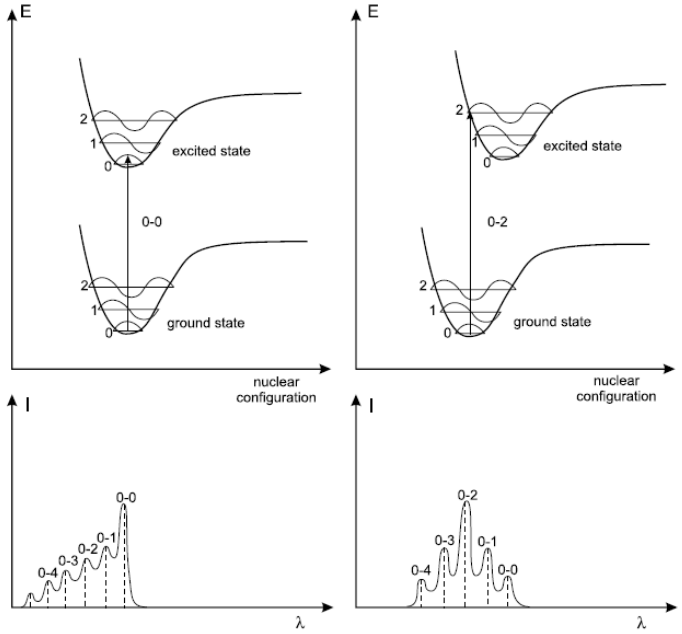

Illustration 4: Potential energy diagrams with vertical transition (top). On the bottom the shapes of absorption bands are shown. Dashed lines represent the absorption lines for a vapor whereas solid lines represent the actual spectra. [2]

Illustration 4 shows the Franck-Condon principle. At room temperature, most molecules are in the lowest vibration level. The bandwidth in the absorption spectrum is a result of two effects, namely *(i)* homogeneous broadening and (ii) inhomogeneous broadening. The former is due to the existence of a set of vibrational sublevels in every electronic state whereas the latter is due to fluctuations of the structure of the solvation shell.

2.1.2. Fluorescence emission – Characteristics

2.1.2.1. Perrin-Jablonski diagram

The Perrin-Jablonski diagram is useful for visualizing several processes such as (i) photon absorption, (ii) internal conversion, (iii) fluorescence, (iv) triplet-triplet transition et cetera. Singlet states are denoted by S_i and triplet states are denoted by T_i

with *i = 1, 2, … ,* respectively. A typical Perrin-Jablonski diagram is shown in Illustration 5.

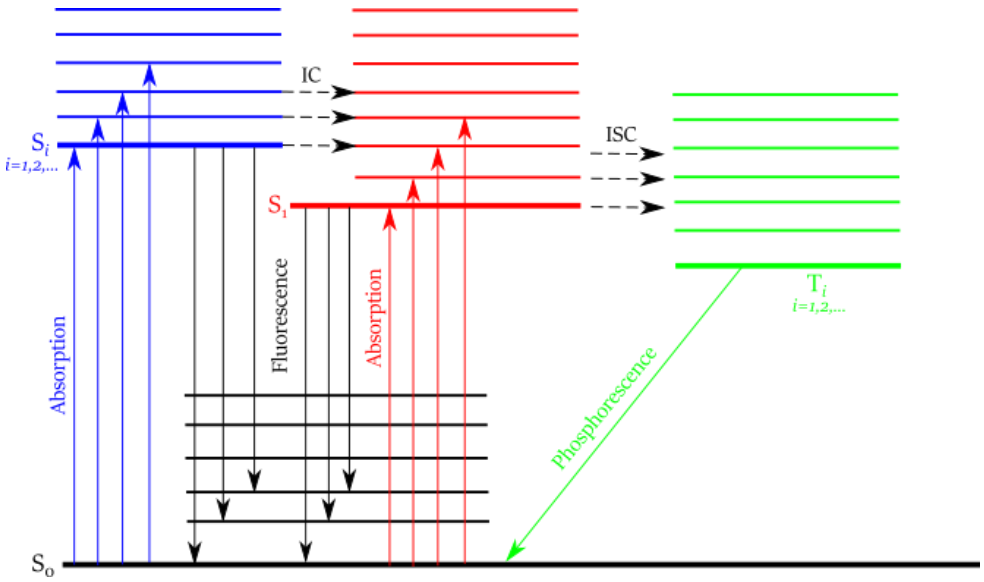

Illustration 5: Typical Perrin-Jablonski diagram with different singlet and triplet states. Black solid arrows represent fluorescence whereas blue and red solid arrows represent absorption. The solid green arrow represents phosphorescence, respectively. [2]

2.2. Optical Sensors [1,4,6–11]

The main reference for this section was [1].

2.2.1. Principles

Measuring chemical quantities in industrial applications, medicine applications or chemical analysis experienced great benefit by using fibre optic sensors and systems. Conversion of the quantity under investigation to an electronic signal is shown in Illustration 6. Reagents are used to recognise the analyte and convert its information into optical properties, e.g. the concentration of the analyte. In the first block, the chemo optical interface, the reagent is immobilised. The chemo optical interface defines the performance and operation principle of the optical sensor. Since the chemo optical interface is in contact with a test sample, it is designed as a membrane which contains reagent molecules. A light source is generated by the electro optical interface which matches to the maximum of excitation of the reagent. The chemo optical interface reflects the light beam and the optoelectronic interface converts the reflected light beam into an electrical signal. The light beam is detected by a photodiode and amplified for further processing. Additional signal processing is done in processing electronics, e.g. microcontrollers.

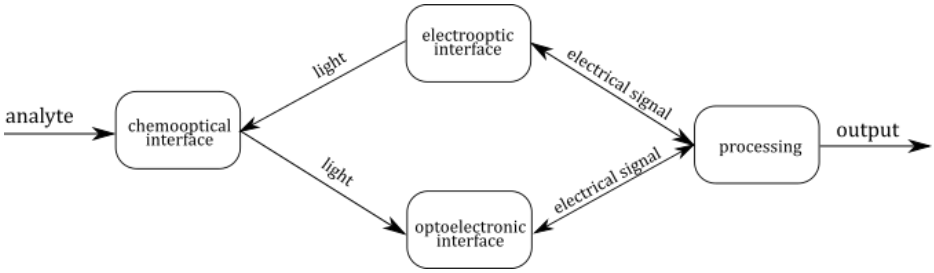

Illustration 6: schematic overview of the basic building blocks of optical sensors [1]

2.2.1.1. Optical Fibres

Optical fibres are the fundamental building blocks to guide light in optical sensors. In chemical sensors, multimode fibres are used about 70% of the time [7]. Multimode fibres are very common due to their capability of transmitting light over short distances and the huge availability of optoelectronic devices on the market. The typical diameter of fibres for chemical sensors lies in the range of 125μm up to 1.5mm. Optical fibres can be made of different materials with its own properties, e.g. (i) silica fibres, (ii) quartz optical fibres or (iii) plastic fibres. Different fibres are used for different ap-

plications and one should carefully choose the correct fibre type. Telecommunication fibres made of silica exhibit high attenuations in the UV range and are not well suited in systems utilising UV radiation. Therefore, quartz optical fibres perform better in such systems. Plastic fibres suffer from high losses but benefit from their elasticity and their high acceptance angle.

2.2.1.2. Connectors for optical fibres

Light attenuation is a very important quantity in optical systems and is caused by interconnections between components. Connectors are therefore optimized to minimize the optical power loss and can be classified into (i) demountable detectors, (ii) splices and (iii) couplers.

2.2.1.3. Light sources

Light sources for optical sensors can be classified into (i) monochromatic sources, (ii) pseudo monochromatic sources and (iii) continuous light sources. Each of these categories has special spectral properties and spectral bandwidths. Sources which emit light in a very broad range are called white light sources, such as gas discharge lamps. In optical sensors, very often xenon arc lamps, tungsten halogen lamps and deuterium lamps are used of this category. Disadvantages are given by their high price and short lifetime and the necessity of wavelength-selecting devices. Pseudo monochromatic devices are for example LEDs. LEDs are very robust and benefit from a very big lifetime. They are made of different semiconductors, such as III-V compounds and pretend the emitted radiation. Emission spectra of LEDs are shown in Illustration 7. Laser diodes can easily be instrumented because they can be modulated by the current. Monochromatic light can be obtained from lasers where especially argon ion lasers are used in many sensors. Various types of lasers are listed in Table 2: Wavelengths of different lasers.

Table 2: Wavelengths of different lasers

Laser	Wavelength [nm]
ruby	694.3
Ar-ion	275-514
Rhodamine 6G	546-640

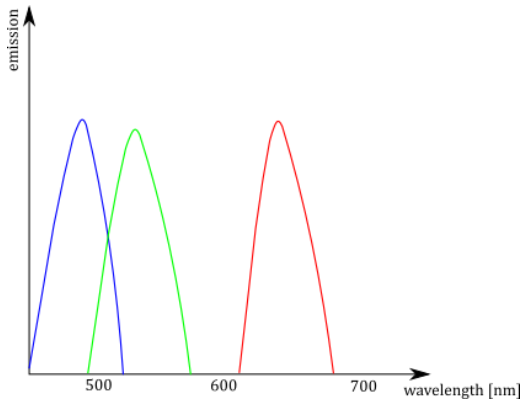

Illustration 7: Typical emission spectra of LEDs. [1]

2.2.1.4. Photodetectors

To obtain an electrical signal, photodetectors convert light into electrical signals. A photodetector is combined with amplifiers and optical elements such as lenses and filters. Detection of single photons can be established by using photomultiplier tubes. They are typically made as a glass tube, which yields a very high robustness against mechanical exposures. Semiconductor-based photodetectors are called quantum detectors. When light interacts with the detector, the conductivity of the detector changes which yields a change in voltage. One of the most used quantum detectors are photodiodes. Additional carrier pairs in the p/n-junction of the diode are generated due to incident light. These additional carriers increase the current in the junction which is proportional to the light intensity. Spectral properties depend on the used semiconductor material in the fabrication process.

2.2.2. Sensor formats

2.2.2.1. Fibre-optic sensors

Fibre-optical sensors are beneficial due to many different reasons. Due to the physical principle, they are robust against electromagnetic interference, are able to perform remote sensing and are highly sensitive in a wide dynamic range. Their material properties also allow usage in high-voltage environments as well as for detection of explosive substances. Today, they are an essential part in medicine application.

The main components are optical fibres, which are dielectric components with cylindrical geometry. They are made of an optical core encapsulated by a cladding with different refraction indices lower than the core. Guidance of light is achieved due to

total reflection at the cladding boundaries. The properties of fibres are given by their attenuation and their numerical aperture NA. The latter describes optical losses due to absorption or scattering of the light, written as

$$\alpha = \frac{10}{L} \log \frac{P_o}{P_i}$$

where P_o, P_i and L are output power, input power and length, respectively.
A typical optical fibre and its principle are shown in Illustration 8.

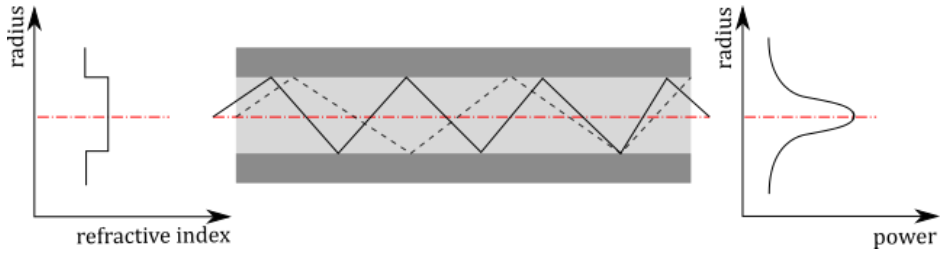

Illustration 8: Geometry of a typical fibre. Dark grey area represents the caddle and light grey the core. The solid line and dashed line represent a light beam. The right plot shows the relationship between radius and output power and left plot of refractive index. [1]

The changes of the analyte can be detected in various frequency ranges such as UV, near infrared, far infrared and visible spectrum. For the UV region, only few materials are sufficient transparent enough. One of the most common materials is pure silica which is suitable for every frequency range. Fibres made of silica benefit from very low losses in the visible spectrum and are ideal for sensing structures. For sensing in IR regions, fluoride glasses are used such as ZBLA or ZBG, Se, Ge-As-Se-systems and many more [8,9]. Contrary to silica fibres, these fibres are complicated to fabricate.

2.2.3. Optical Oxygen Sensors [4]

2.2.3.1. Oxygen sensors based on luminescence

Many oxygen sensors are based on quenching of luminescence of so-called oxygen-sensitive probes (OSPs). Molecular oxygen collides with the excited electronic state of the OPS which yields a reduction of the luminescence intensity and decay time. This dynamic quenching is a fully reversible photophysical process which does not modify the probe and does not distort the absorption spectrum. The main effect lies in a significant drop in luminescence intensity and decay time. A basic equation to explain the relationship between oxygen concentration and decay time is given by the Stern-Volmer equation

$$\frac{F_0}{F} = \frac{\tau}{\tau_0} = 1 + K_{SV}[O_2]$$

where τ and τ_0 are the decay times of the probe in the absence and presence of oxygen, respectively. K_{SV} is known as Stern-Volmer constant and depends on the lifetime of the probe and the solvent. The concentration of oxygen in the sample is denoted by $[O_2]$. One main characteristic of an ideal quencher system is its linearity between the decay time ratios and oxygen concentrations, as shown in Illustration 9.

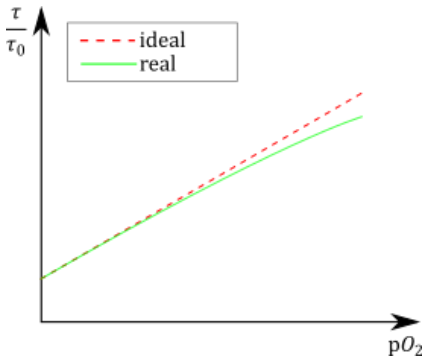

Illustration 9: Stern-Volmer plot. The dashed red line shows the ideal plot whereas the solid green line shows an ideal plot. [4]

Stern-Volmer plots are obtained by measurements of decay times or intensities. The latter suffers from many drawbacks which are mainly given by the poor stability of light sources, drifts in detector sensitivity, inhomogeneous probe distributions and many more. Therefore, it is crucial to use a reference fluorophore to compensate these effects. The detection limits of oxygen sensors are determined by the Stern-Volmer constant which is composed by the initial slope and by the resolution of the instrument.

2.2.4. Other formats of Optical Oxygen Sensors

Basically, one can distinguish between (i) fibre optic sensors, (ii) microparticle based sensors, and (iii) nanosensors.

2.2.4.1. Distributed sensing of oxygen

Distributed sensing enables (i) the localization of zones at the fibre where attenuation occurs and (ii) a quantification of local concentration of chemical species. The latter is performed by measuring the amplitude of variations of the signal. Suppose the luminescence which is emitted by the probe. It seems obvious that it will be emitted through the same waveguide and can be modelled as an acoustic echo. Consequently, one can calculate the distance between source and sensor spot by using the

measured time, with tools from basic physics. The intensity depends on (i) the distance and (ii) on the extent to which the signal is affected by oxygen concentration. The spatial resolution of distributed sensors is compromised by the decay time of a probe. There has to be remarked that long lifetime probes will not allow good spatial resolutions and most decay times are given around 20 ns, they are mostly preferred for high spatial resolution. If probes have larger delay times, one can space the sensor regions closer. This is accomplished by using a second fibre as an optical delay line.

2.2.4.2. Microparticle-based sensing

This type of sensor is mainly used as a bulk material. Due to their size, they are not really used for intracellular sensing, because they are mostly larger than the cell. The sensors can be prepared by polymerization or precipitation.

2.2.4.3. Microsensors

This type of sensor consists of a micro-sized semiconductor which is covered with oxygen-sensitive coating. The semiconductor acts as a light source for photoexcitation as well as a support. The sensitivity is comparable to that of ruthenium-based sensor systems. Microsensors are in general very compact and intriguing due to the integration of semiconductor components. An application would be the sensing of oxygen and pH values in parallel by using embedded microsensor arrays. [4]

2.2.4.4. Nanosensors

Nanosensors are miniaturized oxygen sensors down to about 10 nm radii. This is very beneficial if the application needs small-sized sensors for the measurements. Alsoperturbation, like mechanical or functional perturbations, is basically negligible.

2.2.5. Applications of optical sensors in chemical sensing

A vast amount of applications using optical sensors are available sensing chemical substances. In this subsection, some of them are reviewed.

2.2.5.1. Medicine

Detection of physical and chemical parameters in the human body is one of the main research fields in biomedicine. Therefore, using optical sensors is very beneficial due to the non-invasive measurement principle. The probe remains outside the organism and is placed either on the skin or at a certain distance from the body. Non-invasive

sensors are therefore more easily tolerated by patients and also minimize risks during sensing. Even though optical sensors are very often used in today's medicine, invasive sensors still exist and invasive applications at humans are still necessary.
Some examples in medical applications are given for detection of enterogastric and non-acid gastro-oesophageal refluxes [10] which are known as bile sensors. Also monitoring of blood-pH and detection of pO_2 and pCO_2 are crucial in medical applications [11], e.g. at care units. Fibre optical sensors can provide continuous monitoring and are therefore widely used.

2.2.5.2. Measuring Optical Gas

Gas sensors are important for industrial, medical and environmental applications. Detecting gas is divided into (i) direct and (ii) indirect methods. Monitoring optical emission or absorption of gas at defined wavelengths is possible with optical sensors. Spectroscopic methods are fast, stable and accurate for suitable bandwidths. Optical fibres are for example used for remote gas detection applications in harsh environments.

2.2.5.3. Cultural heritage

In artwork, damages can be detected using Laser Induces Breakdown Spectroscopy. Thus, optical methods can give insight into artwork due to different colour pigments which results in different intensities. For example, old manuscripts can be analysed in the IR spectrum and the resulting IR image could be better readable as the original manuscript in the visible frequency spectrum.

2.3. Microfluidics [2,12–18]

This section deals with the description of microfluidic systems. First and foremost, theoretical principles of microfluidics are introduced which are mainly based on fluid mechanics. Afterwards, micropumps, detection methods and application of microfluidics are described. Most of the content was taken from [2].

2.3.1. Overview

Microfluidics is the processing of small amounts of fluids using channels with dimensions in the micrometre range. Microfluidics are very often used in so-called lab-on-chip technologies with the goal to develop an entire laboratory on a single chip. The basic principles of microfluidics are given by fluid mechanics and the ability to integrate electronic circuits at submillimetre level. Such systems are abbreviated as MEMS (microelectromechanical systems) and combine both electronic and mechanical systems on a chip.

There are two basic principles behind microfluidics, (i) analogy microfluidics which use continuous flow and (ii) digital microfluidics which use finite flow, e.g. droplet based approaches. The motion of the fluid can be achieved with mechanical or pressure pumps and due to surface tension effects or electrostatic phenomena [16]. Various lab-on-chip techniques [17,18] enabled successful microfluidic applications. Lab-on-chip approaches benefit from the reduced sample size which allows very fast analysis and efficient detection methods.

2.3.2. Scaling laws

Scaling laws are used to explain the physical properties of microsystems by expressing the variation of physical quantities, such as time or pressure, with the system size l. A major insight is the scaling law of surface forces and volume forces. The gravity force for instance is one of the predominant forces for macrosystems and can be neglected in microsystems. This can be shown by the scaling law which yields,

$$\frac{F_S}{F_V} \propto \frac{l^2}{l^3} = l^{-1}$$

Table 3: Phenomena and their importance in macro- and microchannels

Phenomenon	Macrochannels	Microchannels
Gravity	Dominant	Negligible
Reynolds number	Laminar and turbulent flow	Laminar flow
Surface tension	Negligible	Dominant
Diffusion	Negligible	Important
Surface roughness	Negligible	To be considered

where F_S is the surface force and F_V is the volume force. By decreasing the size, one can observe that surface forces turn out to be the predominant part in microsystems [2]. To give an intuition about microchannels and macrochannels, Table 3 lists predominant flows, respectively.

2.3.3. Fluid Motion

2.3.3.1. Definition of a Fluid

In general, one can distinguish between two types of fluids, namely liquids and gases. They only differ by their densities and by the degree of interaction between molecules. Given ambient temperature, real gas densities are low and molecule motion can be modelled by free particles. On the other hand, liquids behave more like solids. Thus, molecules achieve a very high density and therefore a very low intermolecular distance results. The main difference between the liquid and an actual solid is that liquids can be deformed continuously. For any given action, the fluid responses with a time-dependent deformation which will be defined as the flow. The viscosity for liquids is the property with major importance.

One can explain viscosity by considering two parallel planes of surface A with the top one sliding at velocity v_0, exemplified in Illustration 10. Due to the plane motion, the fluid below will also start to move which is known as *Couette flow.* The friction force F on the surface plane is then proportional to the velocity variation form one plane to the other which can be expressed by a differential equation

$$\frac{F}{A} = -\eta \frac{\partial v}{\partial z}$$

The material constant η is known as dynamic viscosity (unit = Pas) and the ratio $\frac{F}{A}$ is called shear stress. For small viscosity, the fluid motion and the shear stress are very low or even vanish.

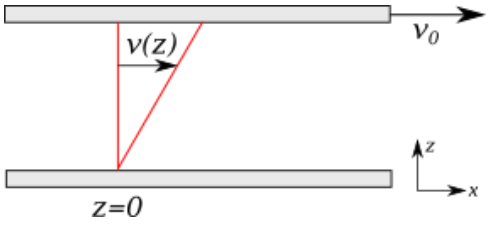

Illustration 10: Modelling of the movement of a plane and fluid to describe the properties of viscosity [2]

2.3.3.2. Acceleration of Fluid Particles

To explain the acceleration of fluid particles, consider a particle with volume V in a given geometry, as shown in Illustration 11.

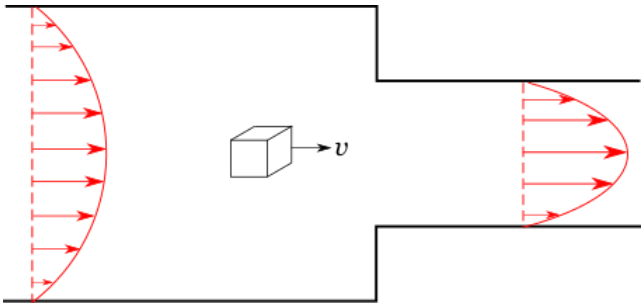

Illustration 11: principle of acceleration of fluid particles [2]

The velocity vector depends on time and position, thus one has a function which depends on 4 parameters $\boldsymbol{v}(x(t), y(t), z(t), t)$. To evaluate the acceleration, one has to evaluate the partial differentials of the velocity vector. By doing so, one obtains

$$\boldsymbol{a} = \frac{\partial \boldsymbol{v}}{\partial t} + (\boldsymbol{v} \cdot \boldsymbol{\nabla})\boldsymbol{v}$$

where $\boldsymbol{\nabla}$ is the Nabla operator. The second term describes the increased velocity due to mass conversation. For the mass conversation, consider a volume V bounded by a closed surface S. By assuming a stationary surface, one can state that at every moment, the change of the total mass is opposite of the outgoing flow through the surface. This leads to the continuity equation

$$\frac{\partial \rho}{\partial t} + \nabla \cdot (\rho v) = 0$$

where ρ is the density of the fluid. If the fluid is incompressible one observes

$$\nabla \cdot v = 0$$

which is clear, due to the constant density.

2.3.3.3. Surface Forces

The shear is defined as the force acting on the surface of a fluid element. If the fluid is at rest, the shear equals the hydrostatic pressure and is normal to the surface. When the fluid moves, stresses appear parallel to the surface due to friction between different layers of fluid. These fluid layers come from the fluid viscosity. Considering

$$\boldsymbol{\sigma} = \begin{pmatrix} \sigma_{xx} & \sigma_{xy} & \sigma_{xz} \\ \sigma_{yx} & \sigma_{yy} & \sigma_{yz} \\ \sigma_{zx} & \sigma_{zy} & \sigma_{zz} \end{pmatrix}$$

the fluid element as an infinitesimal small cubic volume, one can define 9 stresses which are merged into the stress tensor $\boldsymbol{\sigma}$ which can be written as a matrix.

Note that the diagonal elements correspond to normal stresses whereas non-diagonal elements are parallel stresses.

2.3.3.4. Navier-Stokes equation

Newton's second law for a liquid is given by

$$\rho \frac{dv}{dt} = \rho g + \nabla \cdot \boldsymbol{\sigma}$$

where g is gravity acceleration. Using the result of the acceleration and inserting into

$$\rho\left(\frac{\partial \mathbf{v}}{\partial t} + \mathbf{v} \cdot \nabla\right)\mathbf{v} = -\nabla p + \rho \mathbf{g} + \eta \Delta \mathbf{v}$$

Newton's second law one obtains the Navier-Stokes equation

where p is the pressure in Pascal and ∇ is the Laplace operator. Note that this equation assumes constant viscosity of the fluid. The Navier-Stokes equation describes that the time rate of change in linear momentum must be equal to the applied body and surface forces.

2.3.4. Capillary Effect

Given two different fluids, one has to define the interface. The general definition implies an ideal interface which assumes no thickness and smoothness. In the real world the separation of two fluids depends on molecular interactions and on Brownian diffusion. These circumstances are depicted in Illustration 12.

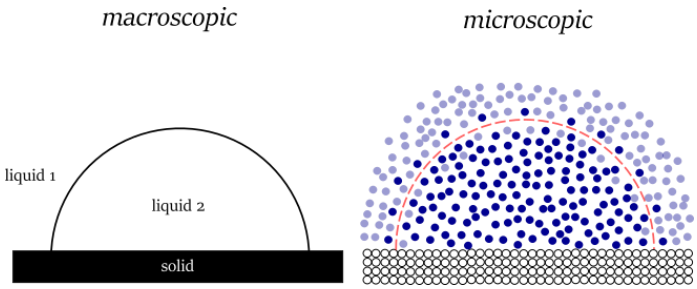

Illustration 12: Interfaces of macroscopic and microscopic level. At macroscopic level, interface is smooth. At microscopic level, molecules interact and Brownian diffusion occurs. [2]

2.3.4.1. Surface Tension

Due to internal cohesion forces which act between molecules of the fluids one can obtain surface tension. Such cohesion forces are given by van der Waals forces, ionic bonds and hydrogen bonding. Therefore, fluids have an elastic tendency known as surface tension. Assuming a liquid-air interface, the tension results from cohesion of liquid molecules. Liquid molecules attract each other greater than molecules of air. The net effect is given as a force at the surface. The liquid behaves like a stretched elastic membrane. This is the reason why water droplets can exist.

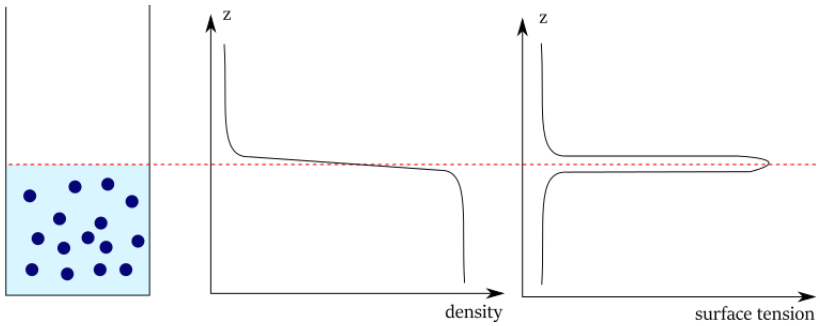

Illustration 13: Relation between fluid density and surface tension for a given interface

2.3.4.2. Capillary length

Effects of capillary are related to the curvature of the interface. At small scales, capillary effects are a significant phenomenon. One can define a length l_c known as *capil-*

lary length beyond which the gravity force becomes the dominant acting force. The capillary length is defined by

$$l_c = \sqrt{\frac{\gamma}{\rho g}}$$

where ρ is the fluid density, g is the gravitational acceleration and γ is the surface tension of the fluid. For water at ambient temperature, the capillary length is typically around 2.7 mm which yields neglectable gravity in microfluidics.

2.3.5. Micropumps

Micropumps are divided into (i) mechanical micropumps and (ii) non-mechanical micropumps.

2.3.5.1. Mechanical micropumps

Mechanical micropumps operate according to mechanical laws of physics. They can be categorized into (i) displacement pumps and (ii) dynamic pumps. In the former, energy is periodically added by force application whereas in the latter, energy is continuously added to increase the fluid velocities within the pump. Examples of mechanical pumps are given by (i) peristaltic pumps and (ii) centrifugal pumps.

2.3.5.2. Non-mechanical micropumps

Non-mechanical energy is converted into kinetic energy without mechanical movement of any structure. Since in microscale environments the fluidic impedance is very high, mechanical pumps cannot deliver enough power. Non-mechanical pumps are very beneficial in microscale environments and use electrical, magnetic, thermal or chemical forces to add momentum to the fluid. Examples are e.g. (i) electrokinetic pumps or (ii) magneto-hydro dynamic pumps.

2.3.6. Applications

Many applications are available were one can use microfluidic systems. One important application is the so-called lab-on-chip system which is widely used. Also, in consumer electronics like inject printers microfluidics are used. In the following subsections some of the most important applications will be discussed.

2.3.6.1. Microreactors

In microreactors chemical reactions take place by injecting at least two fluids separately into the microreactor. Due to diffusion, the fluids will mix together without any

turbulence. The time of the chemical reaction can be obtained by the pressure or the channel length. The advantage of microreactors lies in the improvements in energy efficiency and reaction speed which yields safety and reliable production and a higher resolution of process control. Some other advantages are shorter reaction times and the ability to introduce or extract heat with a very high precision. Also, microcreactor processes are very safe.

2.3.6.2. Lab-on-a-chip

The idea behind lab-on-a-chip is to preserve portable and cheap systems for performing analysis which is currently only available at large labs. Applications are found in wearable health monitoring, where the user can communicate online with the responsible doctor to diagnose disease like cancer more appropriate. Also in military applications like soldier monitoring lab-on-a-chip systems can be used. One can for example implant the chip into the human body for permanent health and stress monitoring.

2.4. Fundamentals of algae- Photosynthesis [19–23]

Algae belong to plant-like organisms which are located in water areas.
Their predominant metabolic reaction, photosynthesis, occurs in presence of light.
In the following reaction equation the involved chemicals are represented.

$$6\,H_2O + 6\,CO_2 + light \rightarrow 6\,O_2 + C_6H_{12}O_6$$

The aim of photosynthesis for plants is the production of glucose or other organic compounds out of carbon dioxide, water and light. Oxygen is actually a by-product of this reaction.
Principle of photosynthesis is the formation of energy-rich compounds out of low-energy educts by the energy of light.
The underlying principle of photosynthesis is the union of light reaction and dark reaction, the so called Calvin cycle. The light reaction described above could only occur, due to the fact that light-harvesting complexes absorb light. These complexes are chromatophore pigments, especially chlorophyll a is responsible in algae for the light supply of photosynthesis.
As a result of light absorption, chlorophyll a rises to the excited state. When the electron falls down to a lower energy level or to the ground state, energy is released as heat or fluorescence light is emitted. Therefore chlorophyll a has a characteristic absorption and fluorescence spectra for which reason algae could be determined with fluorescence measurements. Most part of the released protons and electrons during light reaction are used in several reaction steps for the production of ATP and NADPH, which are both energy-rich compounds. In detail a chemical potential is formed by transfer of an electron from an excited pigment to an acceptor molecule, which becomes an anion. The electron deficit is balanced by the donation of one electron by a donator molecule. This donator is water, which gets photo-oxidised and the end-acceptor is $NADP^+$, which gets reduced to NADPH. This process is divided into two reactions with an electron-transfer-chain, the so called first and second light reaction. The involved pigment systems are photosystem I and II, which differ in their chemical composition and their redox potential. [22]
Photosystem I consists of hundreds of chlorophyll a molecules, but only one, the reaction centre, is active and has an absorption maximum at 700 nm, why it is also called P_{700}.

Photosystem II has a reaction centre P_{680}. It is responsible for the oxidation of water into two protons and elementary oxygen.

ATP and NADPH are then used during Calvin cycle for the fixation of atmospheric carbon dioxide. Therefore carbon dioxide is integrated into a fivefold sugar, ribulose-1,5-bisphosphate. The build-up instable C_6- sugar decomposes into C_3-complex, 3-phosphoglycerine acid, which is transformed into triose-3-phosphat under reduction of ATP and NADPH to ADP and $NADP^+$. Two molecules of triose-3-phosphate are transformed into glucose.

In conjunction to another important process for algae, respiration should be mentioned. It is the reversal of photosynthesis, due to the fact that oxygen is consumed by the algae. [20]

2.5. Respiration measurements [24–30]

2.5.1. Fundamental Approaches

In contrast to photosynthesis, in respiration oxygen molecules are used as electron sink and water is produced again. The required energy for this process is received by the combustion of the carbon-based compounds which are produced in photosynthesis. The rate of respiration, or also called rate of oxygen consumption, is the drop of oxygen level over time. [26]

The derivation of respiration rates is established by measuring the rate of production or consumption of product or reactant and the determination of oxygen with three principle analytical techniques.

2.5.2. Analytical techniques for the determination of oxygen in water samples [30]

2.5.2.1. Winkler Titration

Winkler Titration is an iodometric method for the determination of dissolved oxygen in water. The Winkler titration was one of the first methods of dissolved oxygen measurements using chemical methods. The basic principle relies on adding manganese sulfate and alkaline potassium iodide in samples of water which results in the production of manganic hydroxide. Since manganic hydroxide is unstable in its natural presence, it combines rapid with dissolved oxygen and produces manganese manganic acid. One of the benefits of iodometric methods is its high measurement accuracy. It is possible to apply iodometric methods to clean water and nowadays it is a classical measurement method of dissolved oxygen. Another property is its low measurement uncertainty given around 0.19mg/L. Drawbacks of the iodometric method are the time intensive procedure. Also, it is not possible to acquire data in an on-line fashion.

2.5.2.2. Clark OXYSENS

Dissolved oxygen in water can be determined due to the diffusion rate of molecular oxygen through a polytetrafluoroethylene film. The oxygen flows through the gas and diffuses to the electrolyte. At the cathode, a reduction reaction occurs and at the anode, an oxidation reaction occurs which leads to a current proportional to the oxygen concentration. Dissolved oxygen can be determined indirectly by measuring the current. At the cathode, hydroxyl ions are produced and to establish charge balance of

the electrolyte solution, chloride ions react with silver at the anode. The measurement time is shorter compared to iodometric methods and benefit from less disturbance. Also, on-line detection is possible and it relies on a simple principle. Note that the electrodes age and contaminated water may damage the electrode.

2.5.2.3. Fluorescence quenching

The basic principles of fluorescence were already treated in this thesis in 2.1.

2.5.2.4. Flux of products and reactants [24]

In this approach the change of reactant, for example O_2, or product, for example CO_2, of respiration is measured over a well-defined period of time, e.g. 12 or 24 hours in the dark. Therefore over the defined period of time consistent water samples need to be taken out of the incubated bottle and measured the chosen reactant with an analytical technique, described in the part above.

Furthermore, the ability for analysing the sample is required during the incubation period. One popular method is the so-called in vitro dark bottle incubation. Dark incubations are a necessity for respiration measurements since concurrent counter fluxes can occur due to photosynthesis. Dark incubations have the ability to eliminate these fluxes.

The bottles are incubated at in situ temperature by holding them in temperature controlled incubators. One problem with the in vitro nature of incubation is the possibility of errors, which motivated in situ measurements of oxygen and carbon dioxide changes to determine respiration.

Limit of detection

Several factors limit the detection of the in vitro approach, such as (i) precision of analytical technique, (ii) replicates number, (iii) ambient concentration and many others. Note that the ambient concentration determines most of the sensitivity since the analytical method works near the practical limits of volumetry. Another important factor is the incubation time which is mainly given by 12 to 24 hours.

3. Materials

3.1. Batch cultures and media preparation: [31]

Algae batch cultures of three algae types were received from Silvia Zieger.

Algae types used: Pleurochrysis elongata (gold algae), Haptophyta
Chlorella vulgaris (green algae), Chlorophyta
Phaedactylum tricornutum (flint algae), Diatom

Illustration 14: Batch cultures of green, gold and flint algae

To avoid contaminations everything needs to be sterilized with 70% ethanol.
Firstly the required media L1 and L1-Si were prepared. Therefore 1L Milli-Q water with 33.4 g sea salt was treated by autoclave for 35 min at 135°C.
Then the stock solutions were added with a sterile filter to the salt-water under a Laminaflow work bench.

Illustration 15: Used Laminaflow

The media were stored in the cold storage room. Following table contains the required stock solutions.

Table 4: Stock solutions for the media L1 and L1-Si

Substance	**Concentration [g/L]**	**Volume for green and gold algae [mL]**	**Volume for flint algae [ml]**
$NaNO_3$	75	1	1
$NaH_2PO_4 \cdot H_2O$	5	1	1
$Na_2SiO_3 \cdot 9H_2O$	100	0	1
Vitamin stock solution		0.5	0.5
Trace metal stock solution		1	1

Table 5: Vitamin stock solution

Substance	Concentration [g/L]
Cyanocobalamin (vitamin B12)	0.001
Biotin	0.001
Thiamine HCl (vitamin B1)	0.20

Table 6: Trace metal stock solution

Substance	Concentration [g/L]
$MnCl_2 \cdot 4H_2O$	180
$ZnSO_4 \cdot 7H_2O$	22
$CoCl_2 \cdot 6H_2O$	10
$CuSO_4 \cdot 5H_2O$	2.45
$Na_2MoO_4 \cdot 2H_2O$	19.90
$H2SeO_3$	1.30
$NiSO_4 \cdot 6H_2O$	2.70
Na_3VO_4	1.84
K_2CrO_4	1.94
$Na_2EDTA \cdot 2H_2O$	4.36
$FeCl_3 \cdot 6H_2O$	3.15

Every 4 weeks half of the algae batch culture needs to be disposed and fresh medium needs to be added afterwards to ensure algal growth.

Daylight lamps are used to illuminate the algae. For 10 h the lights are on and for 14h the algae are kept in darkness.

3.2. Used devices

Table 7: Used devices

Device	Manufacturer
Microfluidic rhombic chamber chips	ChipShop
Syringe pump	TSE Systems
pump	Tecan
Lamina flow workbench	Lorica Lamsystems
Microscope Axiovert 25	Carl Zeiss
FirestingO2	Pyro Science
fluorescence spectrophotometer F-7000	Hitachi
Sensicam	PCO
Microdispenser MDV 3200A-HS-UF	VERMES

4. Experimental Part

4.1. Setup for cultivation of algae

4.1.1. Seeding experiments of algae in microfluidic chips:

The algae were grown for first experiments in microfluidic rhombic chamber chips with a volume of 250 µl and a channel depth of 800 µm.

Three approaches were implemented for the seeding of algae in microfluidic chips:

a) seeding of the three algae in open chips in a petri dish (picture bel-low)
b) seeding in open chips with a sensor spot, closed before filling with algae
c) seeding directly in a closed chip

Approach b) and c) were at first only prepared for the gold algae. Approach b) was used for further algal growing experiments in microfluidic chips.

The used oxygen sensor spots were cut from a sensor foil of pyro science.

Illustration 16: Cultivation of algae in open chips inside petri dishes

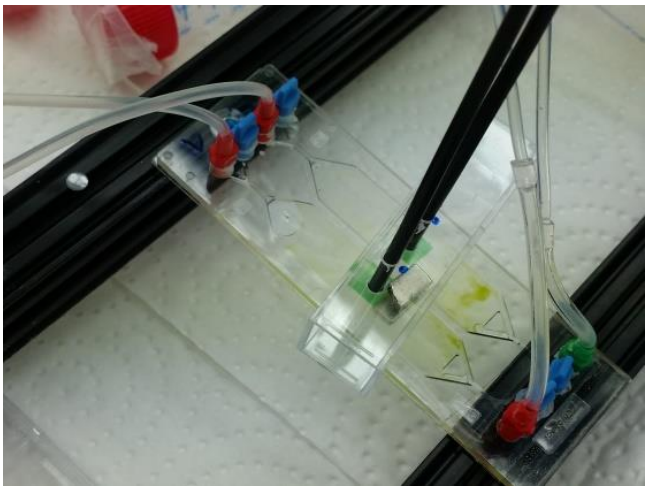

Illustration 17: Chip with oxygen sensor spots

The algae were seeded three days in the chips without media flow. After that the open chips with green and gold algae were closed. The added medium volume was 30 µL every 6 hours for every chamber (with a flow rate of 1.2 µL/min). For this experiment one chamber with gold algae was served with a continuous medium flow of 5 µL/h with a syringe pump.

In the following picture (see Illustration 18) the whole setup with the tecan pumps can be seen.

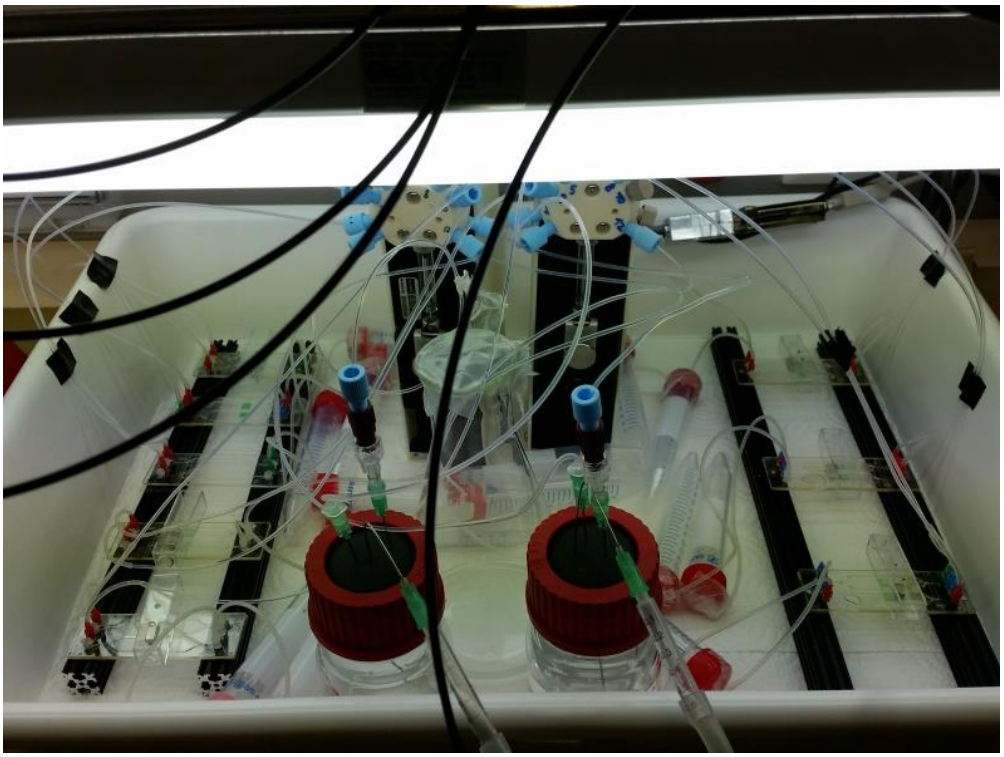

Illustration 18: Setup for the cultivation of algae in microfluidic chips (800 µl rhombic chamber chips)

Cell counting on the microscope and taking photos of the cells was also tested.

Cultivation in 250 µl rhombic chamber chips:

The added volume was adjusted to 5 µL/h in semi-continuous mode with a flow rate of 1.2 µL/min. That was done to get a supply of the algae in nearly similar condition to the continuous flow of the syringe pump.

4.2. Evaluation of flow rates

Flow experiments with a syringe pump were done to test faster possible flow rates. First the Pleurochrysis elongata (gold algae) were tested with flow rates starting at 5 µL/h up to 800 µL/min. The same procedure was done for Chlorella vulgaris (green algae) and Phaedactylum tricornutum (flint algae).

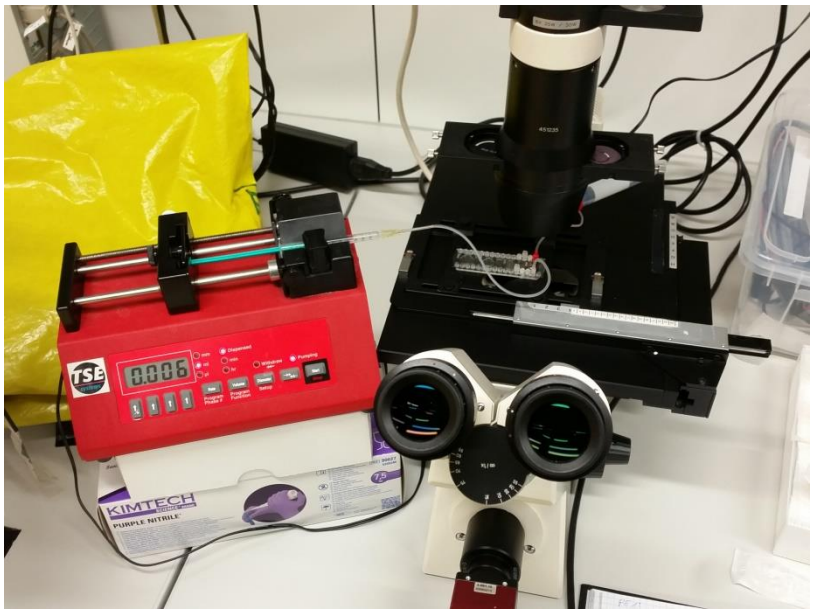

Illustration 19: Evaluation of flow rates on the microscope with a syringe pump

After these experiments the added medium volume for the 250 µl rhombic chamber chips was increased to 62.5 µL/h, semi-continuously 62.5 µL in about 5 minutes with a flow rate of 12.5 µL/min.

4.3. Microscopic determination of cell fluorescence and cell number [3,5]

Different chamber sizes and volumes were tested under the microscope for cell counting (250 µl, 60 µl, 20 µl, 10 µl).

The 10 µl rhombic chamber chips were chosen for further experiments because of a good overview through the chip with only three positions to measure.

4.3.1. Routine for the measurements on the microscope

10µL rhombic chamber chips were filled with the algae solution. Pictures were taken at three positions of the chip: (i) the middle of the chamber, (ii) on the side of the inlet and (iii) on the side of the outlet.

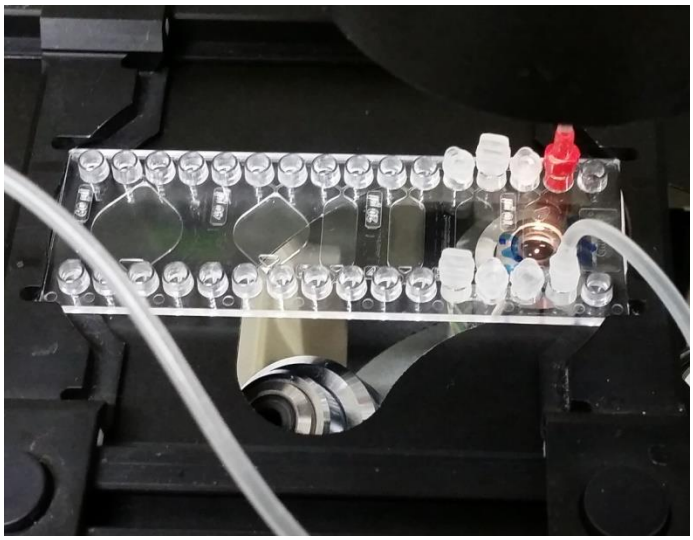

Illustration 20: Chip on the microscope for cell counting and fluorescence measurement

Taking pictures of the chips followed the procedure below:

- At optical magnification of factor 20 the picture was focused.
- First 10 minutes waiting in the dark.
- 5 seconds of light by the HBO lamp (through the filter cube to the chamber)
- One fluorescence picture was taken.
- 3 pictures with transmission light were taken.

The same procedure was also done for all positions.

The cells were also counted in the cell counting chamber (Thoma neu) as reference.

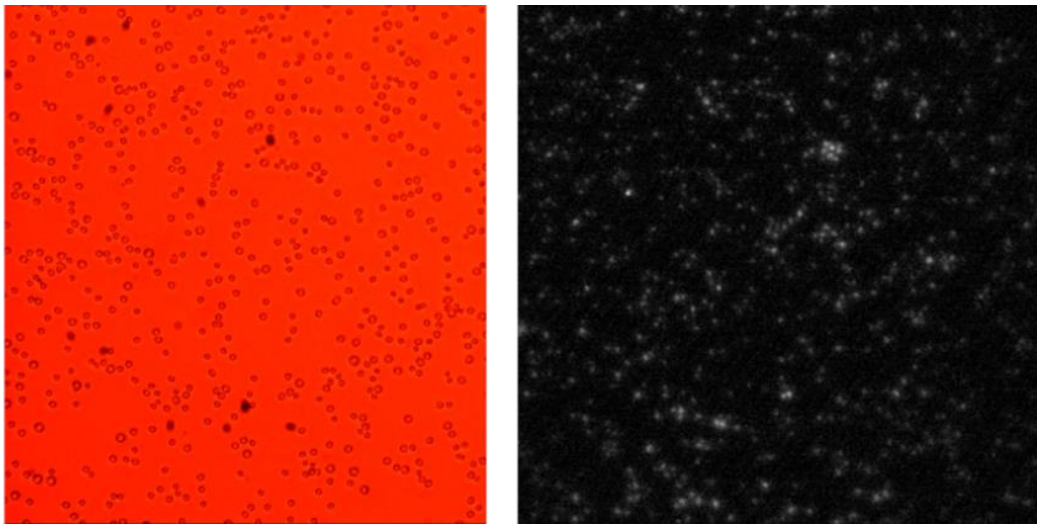

Illustration 21: Transmission picture and fluorescence measurement picture

4.3.2. Reference measurements on a fluorescence spectrophotometer

To get comparable and controllable fluorescence data the chambers and also 2 ml of the algae solution in a cuvette were measured on the Hitachi fluorescence spectrophotometer F-7000 with excitation at 363 nm and emission at 450-900 nm.

Into the light path the filter RG665 was integrated because otherwise the 2nd order of the excitation wavelength could be seen in the fluorescence spectra. The signal intensity was taken at 680 nm, because algae spectra have maxima at 363 nm and 680 nm.

For a reliable calibration curve five dilutions were made out of one concentrated green algae solution. Therefor 15 ml algae batch solution was centrifuged and half of the supernatant was removed out of the tube. This concentrated stock-solution was used for the dilutions.

- Blank= medium L1-Si
- concentrated stock solution
- 1.5 ml stock solution + 1 ml medium
- 1.25 ml stock solution + 1.25 ml medium
- 1 ml stock solution + 1.5 ml medium
- 0.75 ml stock solution + 1.75 ml medium

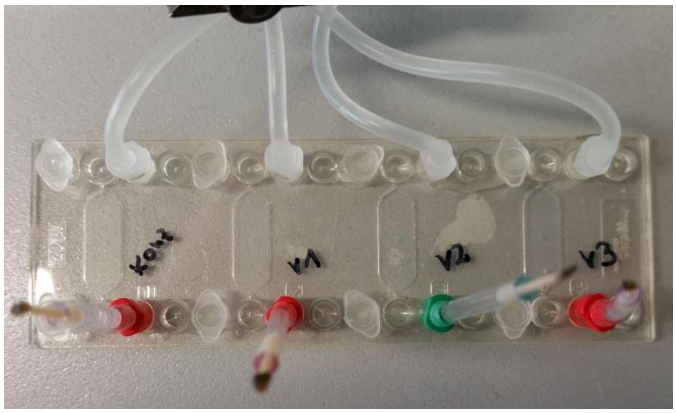

Illustration 22: Calibration solutions filled into the rhombic chamber chip

The solutions were measured in a cuvette and then 10 µl were filled into the small rhombic chamber chips to make transmission light and fluorescence pictures on the microscope.

Evaluation of the photos was performed with the program ImageJ.

ImageJ is an open source image processing program which picture data could be analysed with.

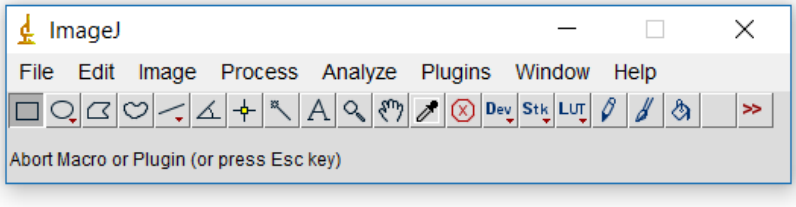

Illustration 23: graphical interface of ImageJ

The raw data, received by a camera on the microscope, was loaded into the program and was converted in red, green and blue part of the picture by function “Debayer Image”. The threshold had to be adjusted on the red part. Then the cells were counted by automatic counting demand.

4.4. Oxygen gradient measurements with a Sensicam

An oxygen nanoparticle suspension was used in dilution 1:10 to make oxygen differences with a blue LED (455nm) as light source visible. Pictures were taken with a sensicam (filter RG9).

Used program settings were: Δ_{ex} = 50 µs

Δ_i = 25 µs

Δ_1 = 1 µs

Δ_2 = 1 µs

Integration time = 500 ms

First experiments were done with the cultivated 250 µl chips with green algae. Media was pumped through the chip with a flow of 12.5 µl/min.

Further examinations were performed in 10 µl rhombic chamber chips, where seeding was done for 3 hours and 1 day. The used flow rate for these chips was 1 µl/min.

Because of bad handling in the 10 µl chips the experiments were also undertaken in 20 µl chips.

Because of the good handling with the 20 µl chips (air bubbles can be get out) they were used for further experiments.

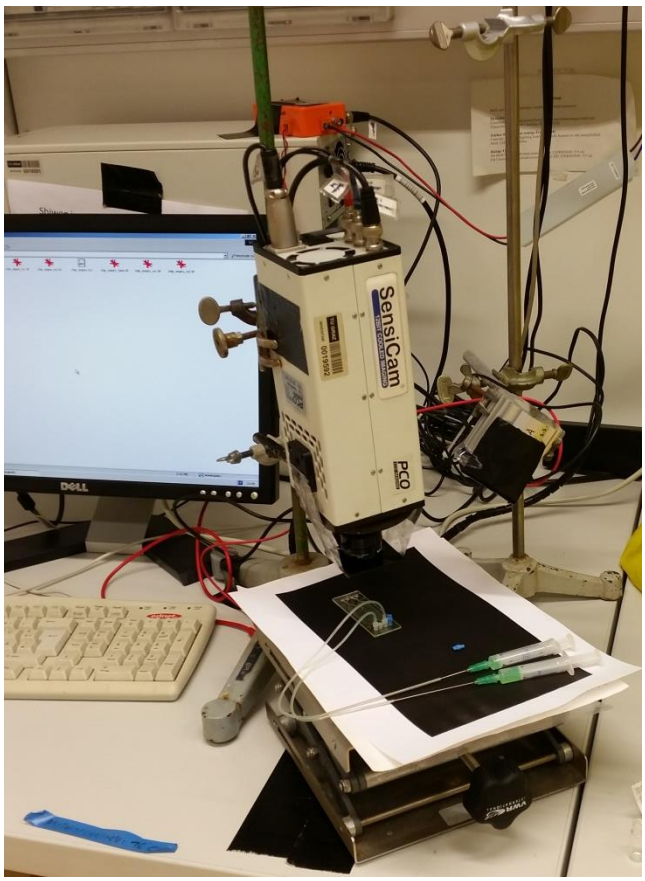

Illustration 24: Setup for measurements with the sensicam

4.5. Relationship between the gradient of pO_2 and cell number

For the last part of experiments for this master thesis a reduction in chip volume to 20 µl was made. Into the first generation of these chips three small oxygen sensor spots were integrated (Inlet, Middle, Outlet).

The integration was undertaken by spotting with a micro dispenser produced by Vermes. The used software is Python 3.2.

The O_2- mix for spotting was developed by Nicola Altenhuber. The mixture contains 6% D_4 in isopropanol: water 9:1. 750 mg of that were taken for creation of the spotting solution with 47.9 mg O_2- particles (Pt_4Br_8Cl in polystyrol).

Micro dispenser adjustment:

- 70 µm nozzle
- 0.4 bar
- tappet lift: 65
- rising time: 0.3
- open time: 0.1
- falling time: 0.1
- delay: 0.1
- number of pulses: 3

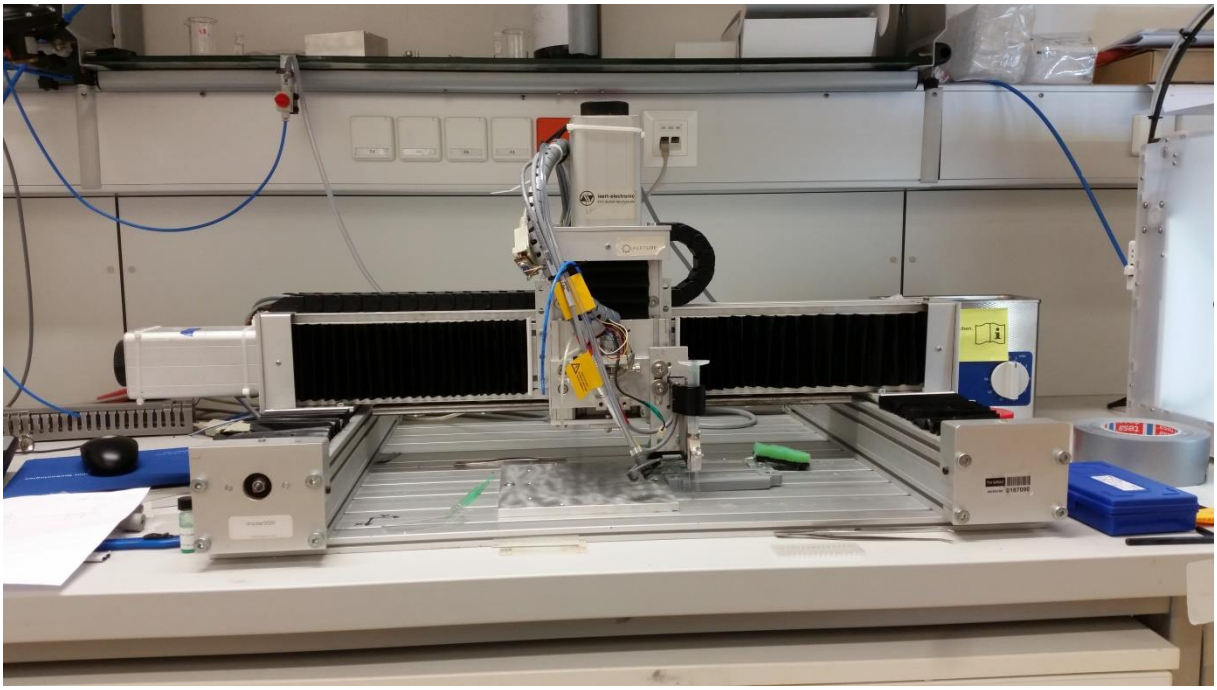

Illustration 25: Micro dispenser, produced by Vermes, used for spotting of oxygen sensor spots into the microfluidic chips

Illustration 26: 20 µl rhombic chamber chips for the examination of the conjunction between the fall of pO_2 and cell number

After evaluation of the first experiments next generation of chips only had one spot in the middle integrated for oxygen measurements.

Oxygen measurements were always taken at nearly the same time of the day (noon) and oxygen data was plotted for the first 10 minutes in the darkness.

Cell counting was always performed after the oxygen measurements with 20x magnification and between the sensor spots (means on left and right side of the middle spot).

5. Results and Discussion

The main question of this thesis was if the cultivation of algae in microfluidic chips is possible. The integration of oxygen sensor spots into the microfluidic chips worked well and filling of the chambers with algal solution was realised with small flow by hand. All seeding tests with the algae in the rhombic chamber chips showed that the cultivation of algae in microfluidic chips is possible and sufficient oxygen supply in microfluidic chips is ensured. This could be observed in increasing oxygen production during light phase and a drop of oxygen level during the dark phase.

Also small air bubbles occurred in the chips due to algal respiration and production of oxygen. The bubbles could be pressed out through the chips from inlet to outlet when the microfluidic chip was stored in slightly angular state during addition of medium.

Therefore could be stated that algae grow in microfluidic chips and their monitoring by optical oxygen sensor spots was carried out successfully.

Illustration 27 and Illustration 28 show the green algae on two different dates, the first picture was taken after 3 weeks of cultivation in the microfluidic chips, the second one after three months. Already small areas of intense vegetation could be observed. The growth was located on the inlet side of the chip because with a media supply of 30µL every 6 hours with a flow rate of 1.2 µL/min the nutrition supply was to slow for augmented growth. With a higher portion of added medium volume of 62.5 µL/h, semi-continuously 62.5 µL in about 5 minutes with a flow rate of 12.5 µL/min, the algae cover increased, like on the second picture is depicted.

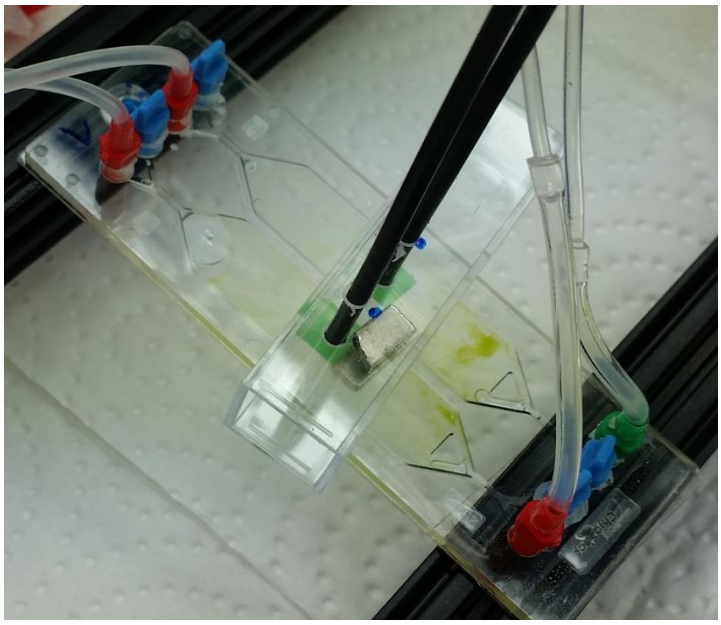

Illustration 27: Green algae after three weeks of cultivation in 250 µl rhombic chamber chips

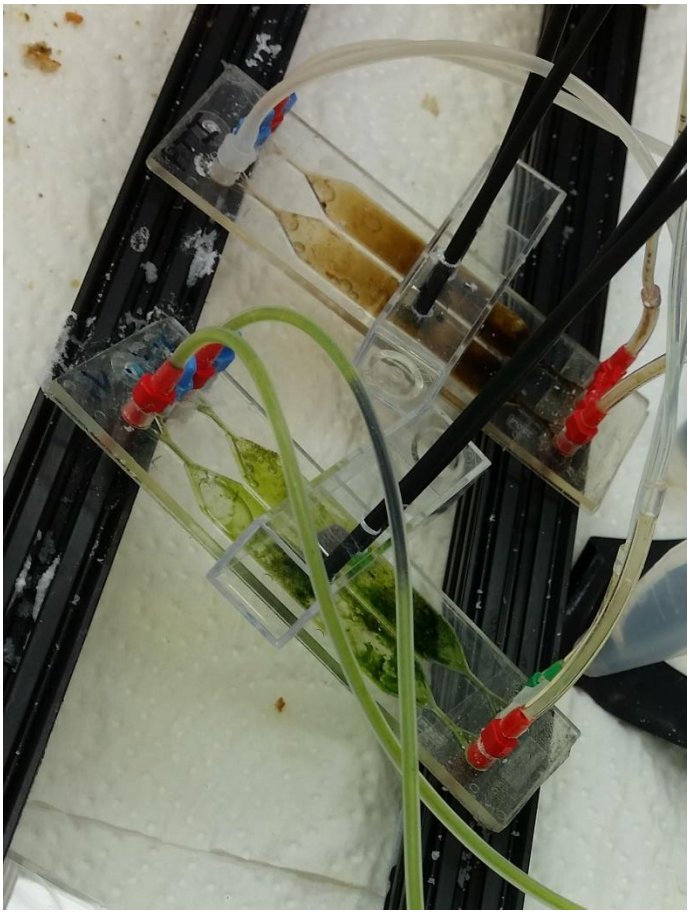

Illustration 28: Green and flint algae after 3 months of cultivation in 250 µl rhombic chamber chips

5.1. Evaluation of flow rates:

Table 8: Maximum flow rate for the three types of algae received by tests with a syringe pump

Algae type	Maximum flow rate
Pleurochrysis elongate (gold algae)	800 [µl/min]
Chlorella vulgaris (green algae)	>900 [µL/min]
Phaedactylum tricornutum (flint algae)	>800 [µL/min]

In Table 8 the maximum flow rates received by tests with a syringe pump are listed. The experiments showed that already at 3 µL/min loose gold algae were washed out and at 800 µL/min also the algae stuck to the walls were washed out. In contrast most algae of the green algae and the flint algae were stuck on the chip walls at flow rates of 800 µL/min. By reason of these different maximum flow rates, the flow rate was increased up to 62.5 µL/h to provide a good media uptake for all algae types. The supply was carried out semi-continuously, 62.5 µL in about 5 minutes with a flow rate of 12.5 µL/min. For flint algae and green algae increased oxygen values were measured after the raise of flow rate (about 500 hPa respectively 300 hPa) and more intense algae growth was observed by a larger algae cover in the chips. In the measurement curve spikes can be seen every hour where the media was pumped into the chip. The problem with big air bubbles was eliminated with faster flow, but nonetheless the higher production of oxygen by the algae leads to some small oxygen bubbles.

5.1.1. Phaedactylum tricornutum (PT)

Following illustration shows the flint algae in the period of day 10 to day 16 after the start of seeding in the microfluidic chips.

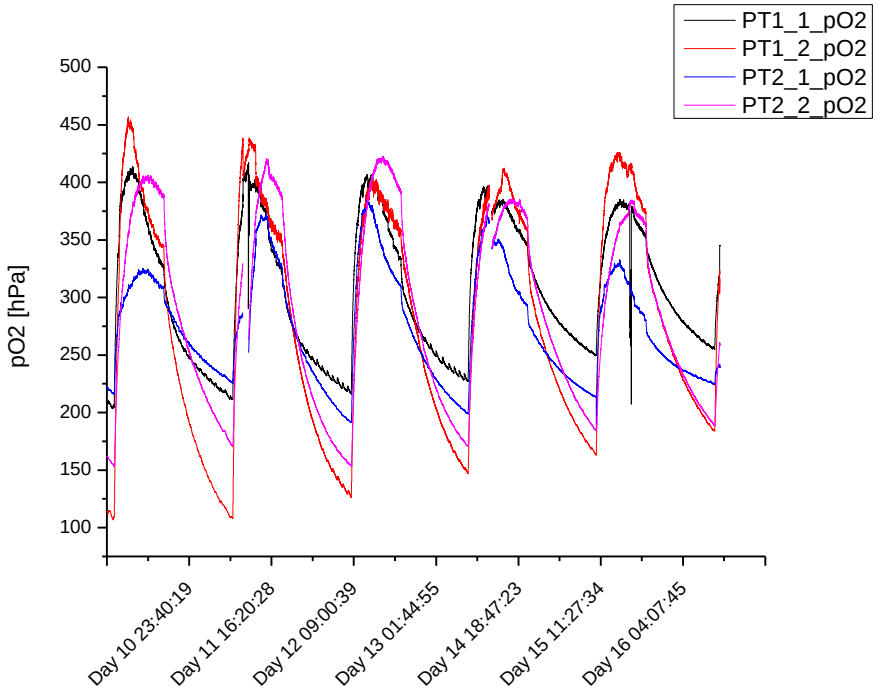

Illustration 29: Oxygen measurement over time with the added medium volume of 5 µl/h for the flint algae, semi continuously with a flow of 1.2 µl/min; day 10- 16 after seeding start. PT1_1: Chip 1, chamber 1; PT1_2: Chip 1, chamber 2; PT2_1: chip 2, chamber 1; PT2_2: chip 2, chamber 2;

In Illustration 29 five peaks up to 450 hPa could be observed. The highest point is the maximum concentration of oxygen reached in this light phase before the light is turned off. The algae had light for 10 hours and 14 hours darkness. The light phase is always combined with a rise of oxygen values in the microfluidic chips. Oxygen values drop during dark phase due to the consumption of oxygen by the algae.

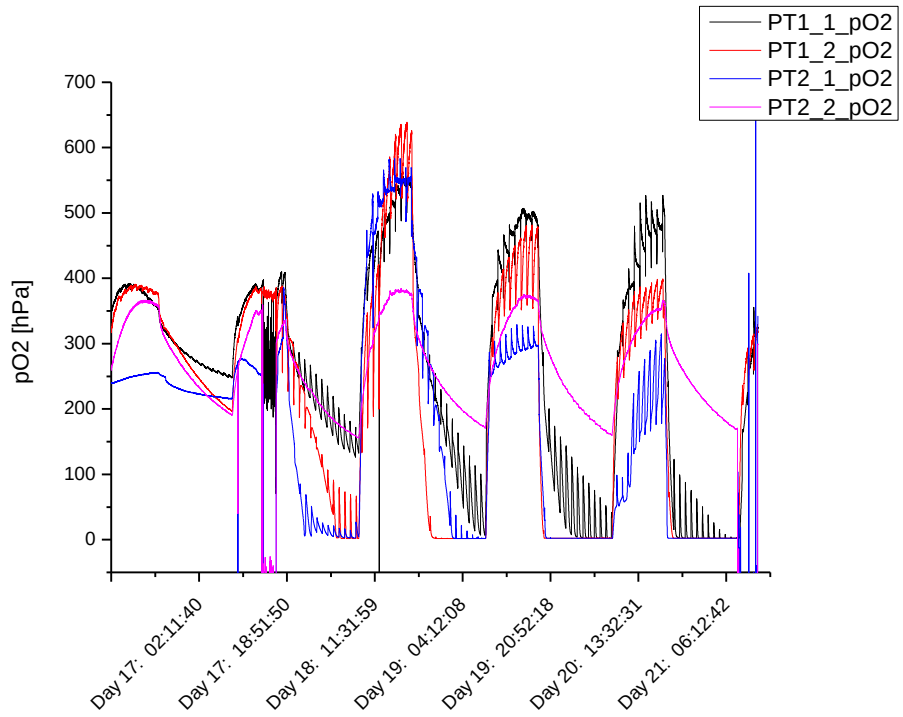

Illustration 30: Oxygen measurement over time with the added medium volume of 62.5 µl/h for the flint algae; semi continuously with a flow of 12.5 µl/min; day 17- 21 after seeding start. PT1_1: Chip 1, chamber 1; PT1_2: Chip 1, chamber 2; PT2_1: chip 2, chamber 1; PT2_2: chip 2, chamber 2;

In Illustration 30 the period of day 17 to day 21 after the start of growing the algae in the microfluidic chips is plotted. The supply of media was increased to 62.5 µL/h semi-continuously, what means 62.5 µL in about 5 minutes with a flow rate of 12.5 µL/min. Every spike in the illustration represents such a media addition.

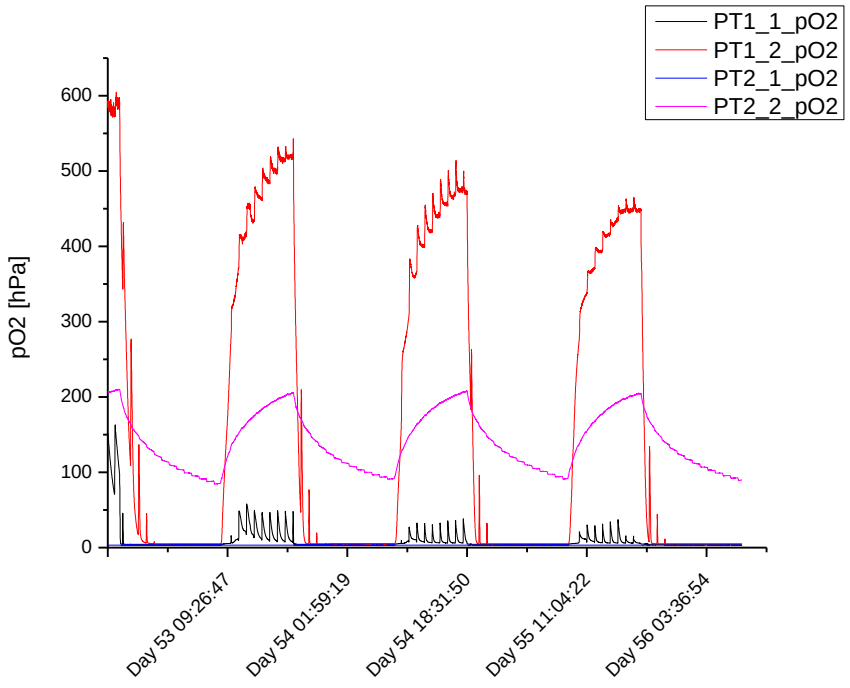

Illustration 31: Oxygen measurement over time with the added medium volume of 62.5 µl/h for the flint algae; semi continuously with a flow of 12.5 µl/min; day 53- 56 after seeding start. PT1_1: Chip 1, chamber 1; PT1_2: Chip 1, chamber 2; PT2_1: chip 2, chamber 1; PT2_2: chip 2, chamber 2;

For the flint algae the values were increasing from the beginning of the seeding until day 53, but from day 53 on the values for 2 chambers dropped to 3-5 hPa. The values of the two other chambers stayed at 290 hPa and 140 hPa for another two weeks respectively. Exact development of the algae during these two weeks could not be determined because of interruption of the measurement by software failure. Bacteria or other microorganisms were found under the microscope in the chambers with dropped to lower oxygen levels than on the experiment start, wherefore a mixture of antibiotics and a fungicide was added to the medium. After two weeks of mixture addition the algae recovered and oxygen values increased.

5.1.2. Chlorella vulgaris (CV)

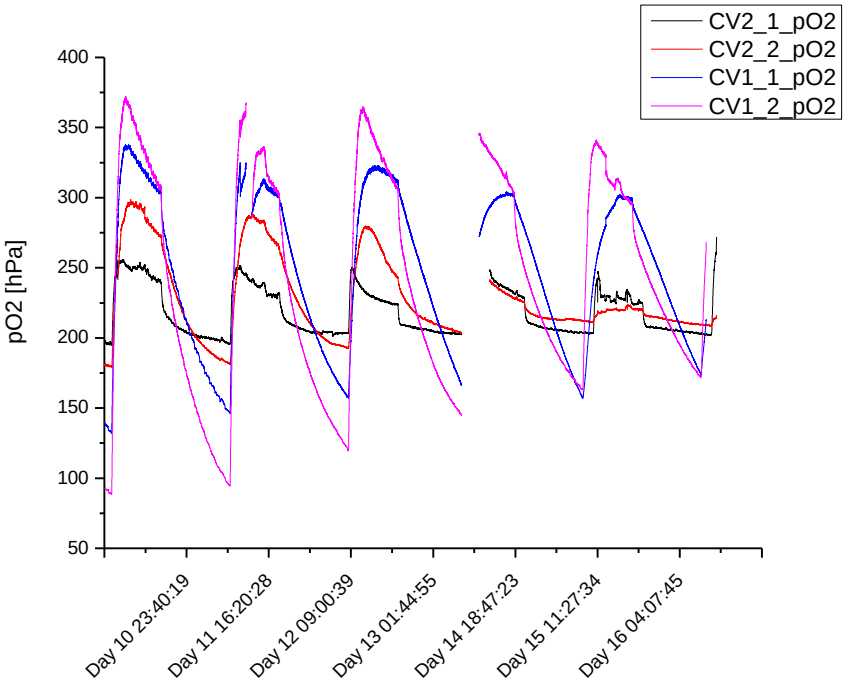

Illustration 32: Oxygen measurement over time with the added medium volume of 5 µl/h for the green algae, semi continuously with a flow of 1.2 µl/min; day 10- 16 after seeding. CV1_1: Chip 1, chamber 1; CV1_2: Chip 1, chamber 2; CV2_1: chip 2, chamber 1; CV2_2: chip 2, chamber 2; the gap resulted from missing measuring data

Illustration 32 shows the oxygen course of the green algae. Like the flint algae the oxygen values rise in light phase and drop in dark phase. The gap in the plot is caused by missing measuring data.

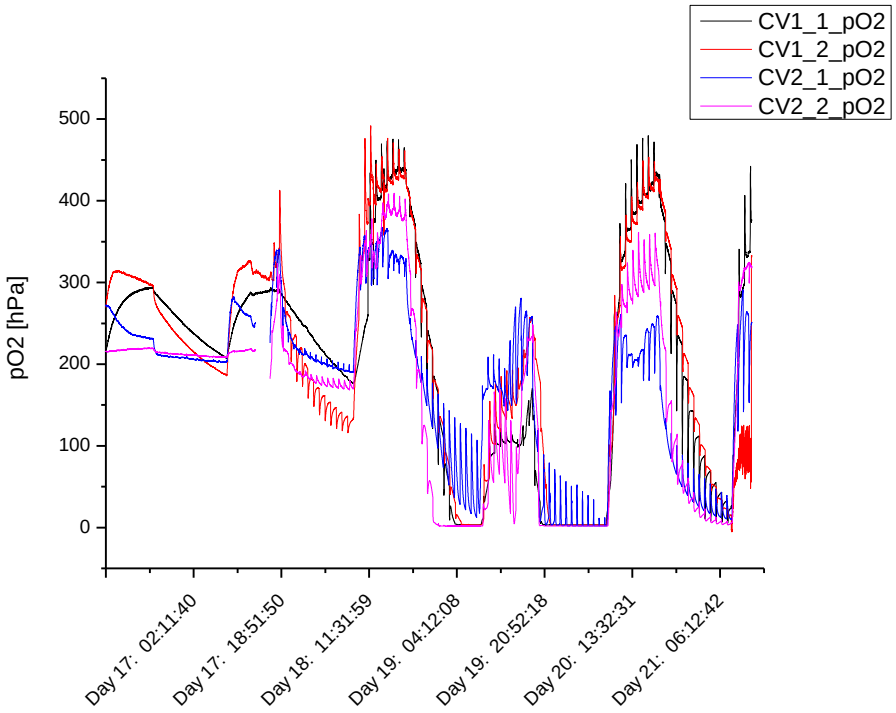

Illustration 33: Oxygen measurement over time with the added medium volume of 62.5 µl/h for the green algae; semi continuously with a flow of 12.5 µl/min; day 17- 21 after seeding start. CV1_1: Chip 1, chamber 1; CV1_2: Chip 1, chamber 2; CV2_1: chip 2, chamber 1; CV2_2: chip 2, chamber 2;

In Illustration 33 the period of day 17 to day 21 after the start of growing the algae in the microfluidic chips is plotted. The supply of media was increased to 62.5 µL/h semi-continuously, what means 62.5 µL in about 5 minutes with a flow rate of 12.5 µL/min. Every spike in the illustration represents such a media addition.

For the green algae the values were most time at about 200 to 400 hPa during day, but low oxygen values of about 5-8 hPa have been measured since day 53. Also the colour of the algae in the chips changed from green to yellow-green since that.

The drop of oxygen values and the change in colour was caused by bacteria or fungi, because two weeks after regular addition of antibiotics/fungicide mixture the algae recovered. This phenomenon could be recognised in an increase of oxygen values and the green algae changed again colour from yellow-green to healthy dark-green.

Illustration 35: Green algae in 250 µl rhombic chamber chip contaminated with bacteria and fungi

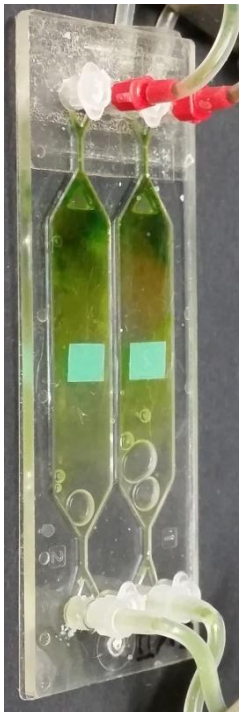

Illustration 34: Green algae in 250 µl rhombic chamber chip after addition of antibiotics for 2 weeks

5.1.3. Pleurochrysis elongata (PE)

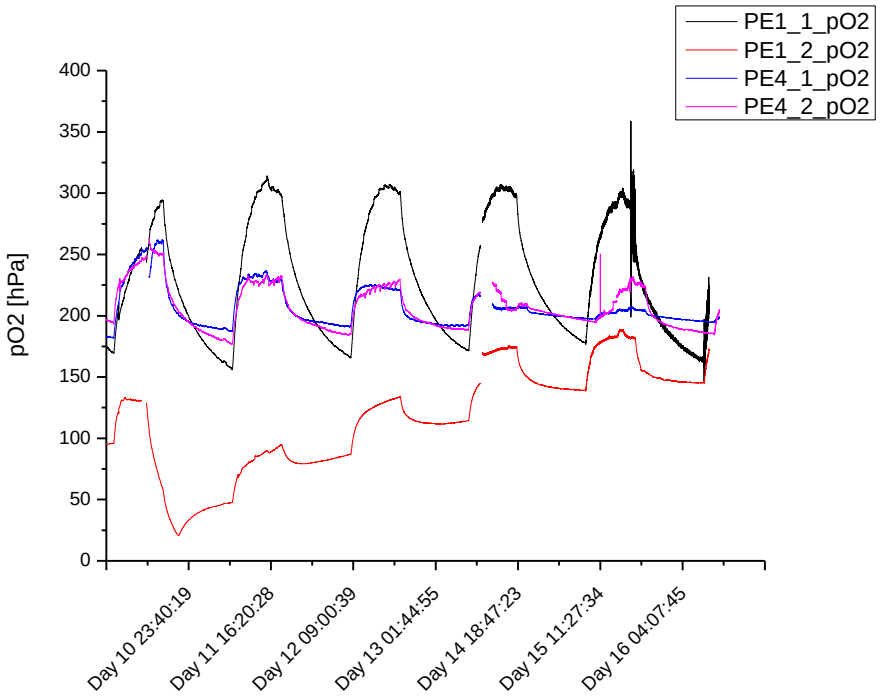

Illustration 36: Oxygen measurement over time with the added medium volume of 5 µl/h for the gold algae, semi continuously with a flow of 1.2 µl/min; day 10- 16 after seeding start. PE1_1: Chip 1, chamber 1; PE1_2: Chip 1, chamber 2; PE4_1: chip 2, chamber 1; PE4_2: chip 2;

Illustration 36 contains the measured data of oxygen values from the gold algae. This algae type stuck less on the chip walls and therefore the algae grew slower which is indicated by less variation of values between light and dark phase.

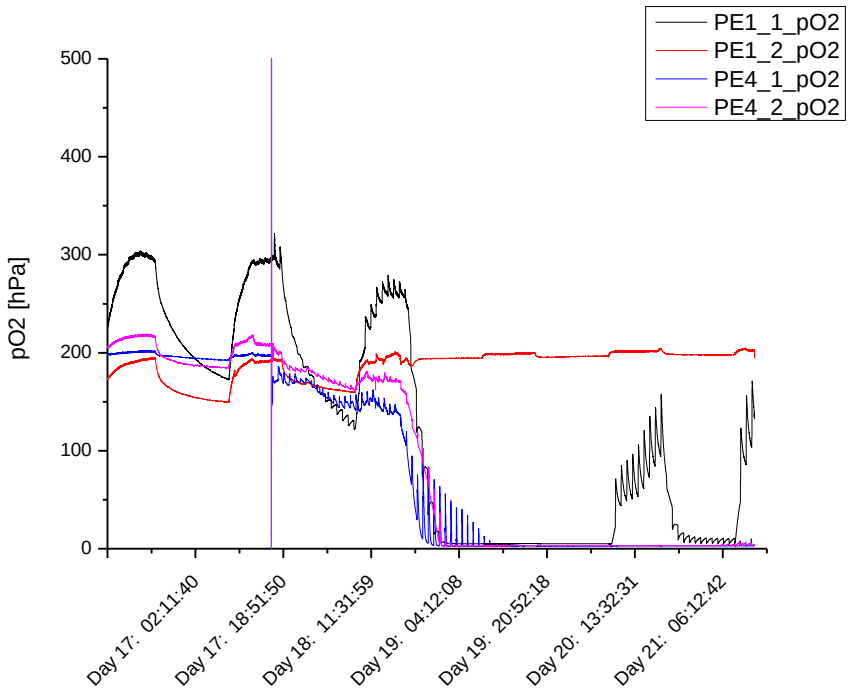

Illustration 37: Oxygen measurement over time with the added medium volume of 62.5 µl/h for the gold algae; semi continuously with a flow of 12.5 µl/min; day 17- 21 after seeding start. PE1_1: Chip 1, chamber 1; PE1_2: Chip 1, chamber 2; PE4_1: chip 2, chamber 1; PE4_2: chip 2; PE1_2 had an air bubble on the sensor spot

Until day 19 after the start of seeding the algae in the chips, the values of the chambers filled with gold algae dropped.

Continuous low oxygen values occurred for the gold algae until day 53.

Also the gold algae had bacteria in their chambers. After addition of the antibiotics the gold algae recovered, but only fewer algae were stuck in the chambers than before the bacteria affection.

5.2. Algal fluorescence measurements

The fluorescence and transmission pictures were taken after the routine described in the experimental part. Evaluation of the cell pictures was done with the program ImageJ. Therefore the average of three counted pictures for every concentration was calculated. As reference the same concentrations of algae were also counted in the cell counting chamber (Thoma neu).

The counted result with the cell counting chamber was received by counting the algal cells under the microscope. The cell counting chamber is composed of 32 small squares which are divided into 2 group squares. An exemplary calculation for the concentration per ml is shown below.

$$99 + 88 + 109 + 105 = 100{,}25 \frac{cells}{groupsquare}$$

$$102 + 99 + 82 + 71 = 87{,}75 \frac{cells}{groupsquare}$$

$$\frac{average\ cell\ number}{groupsquare} = 95$$

$$dimension\ of\ the\ cell\ counting\ chamber = 0{,}0025 * 0{,}1\ mm^3$$

$$\frac{95}{0{,}004\ mm^3} = 23750 \frac{cells}{mm^3} = 23{,}75 *\ 10^6 \frac{cells}{ml}$$

For the automatic calculation of cells/ ml, first the cells were counted on three positions of the microfluidic chip by ImageJ. Then the three received numbers were averaged. The following calculation equation is shown below.

$$\frac{average\ cell\ number}{volume\ display\ window\ [mm^3]} * 10^3 = \frac{cells}{ml}$$

Table 9: conversion factor for the used camera on the microscope

Colorcam	1236x1628 pixel		
Objective	**conversion factor [µm/pixel]**	**Observed area [µm²]**	**Volume display window [mm³]**
10x	0.876	1544120	
20x	0.438	386030	0.077
40x	0.216	93881	

On all results there was only a deviation of 0.4 - 4% for counting with ImageJ in comparison to the cell counting chamber results.

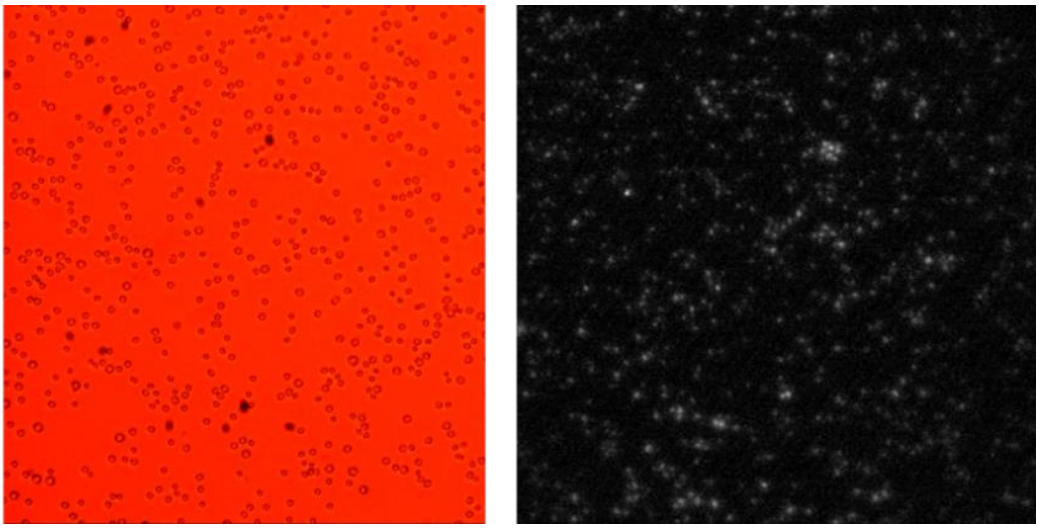

Illustration 38: transmission and fluorescence measurement picture of green algae

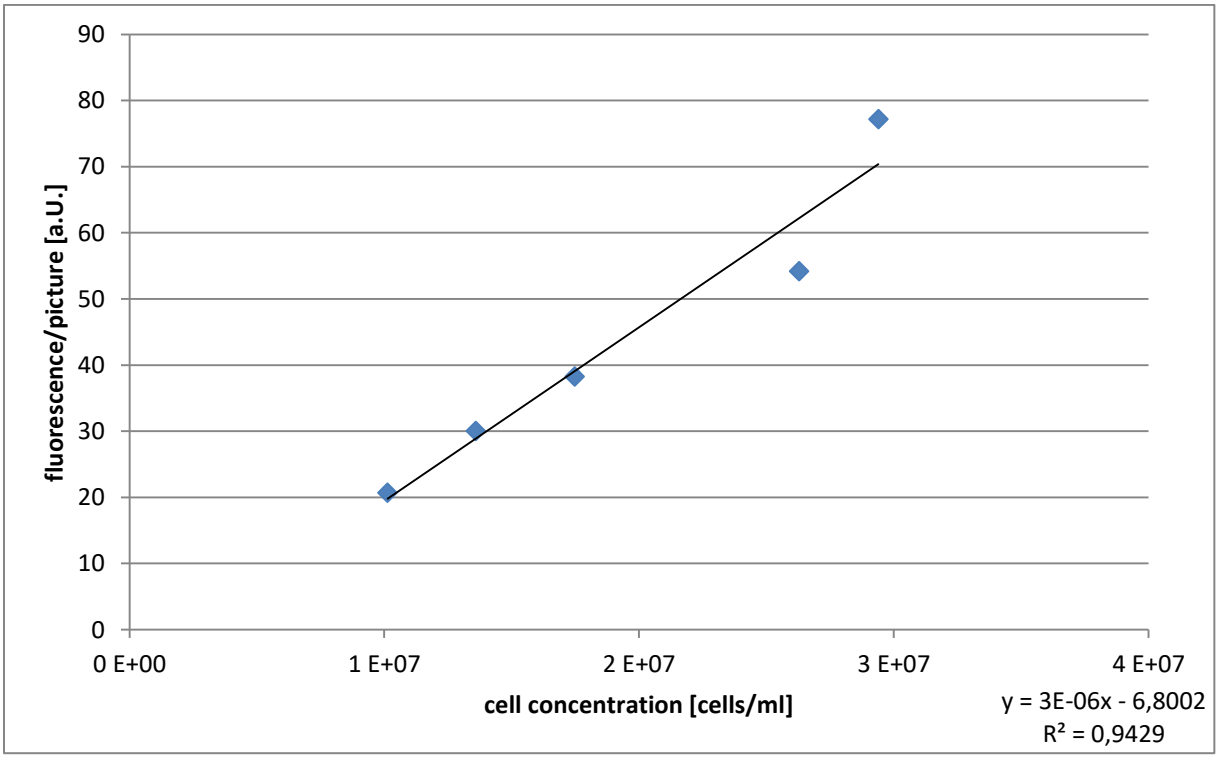

Illustration 39: Fluorescence Calibration of Green Algae on the Microscope

Illustration 39 shows the fluorescence calibration of the green algae with the microscope. The concentrations result in a linear calibration curve. It was not possible to convert the fluorescence per picture into normal fluorescence, but accordance to the fluorescence calibration with the fluorimeter could be given in a linear trend of both measurement methods.

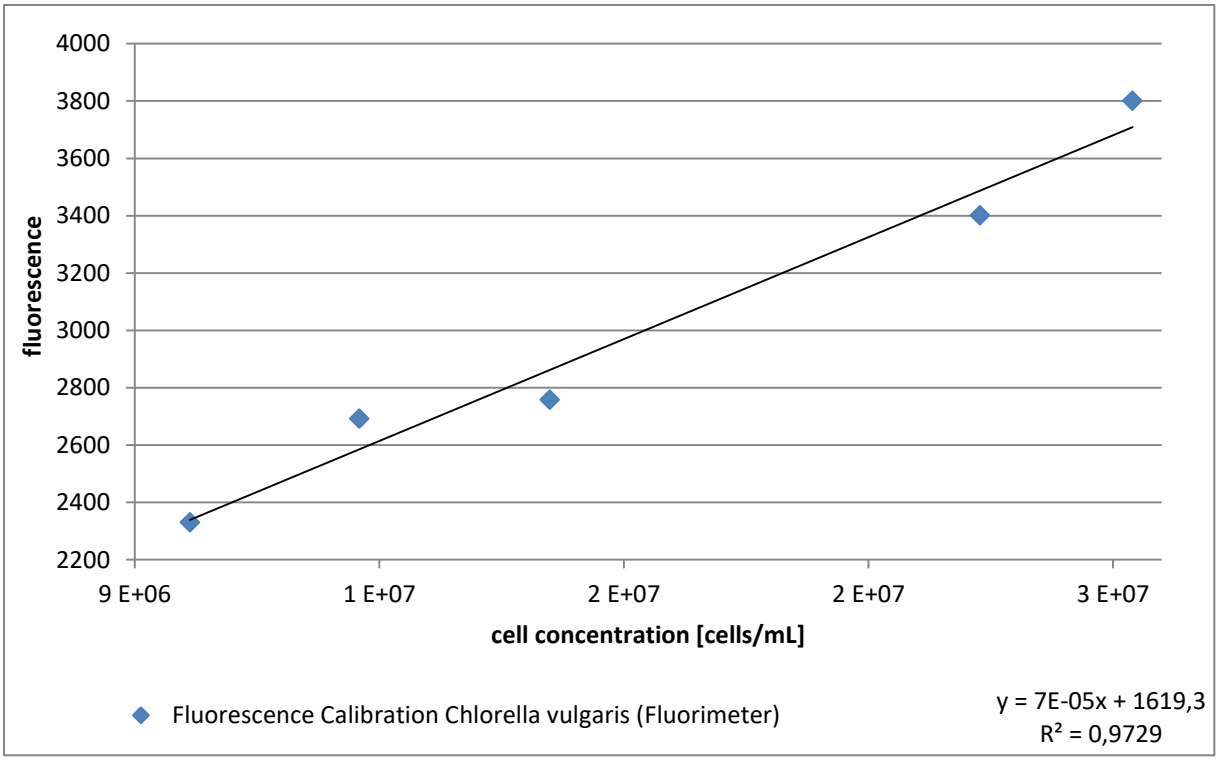

Illustration 40: Fluorescence Calibration of Green Algae on the Fluorimeter

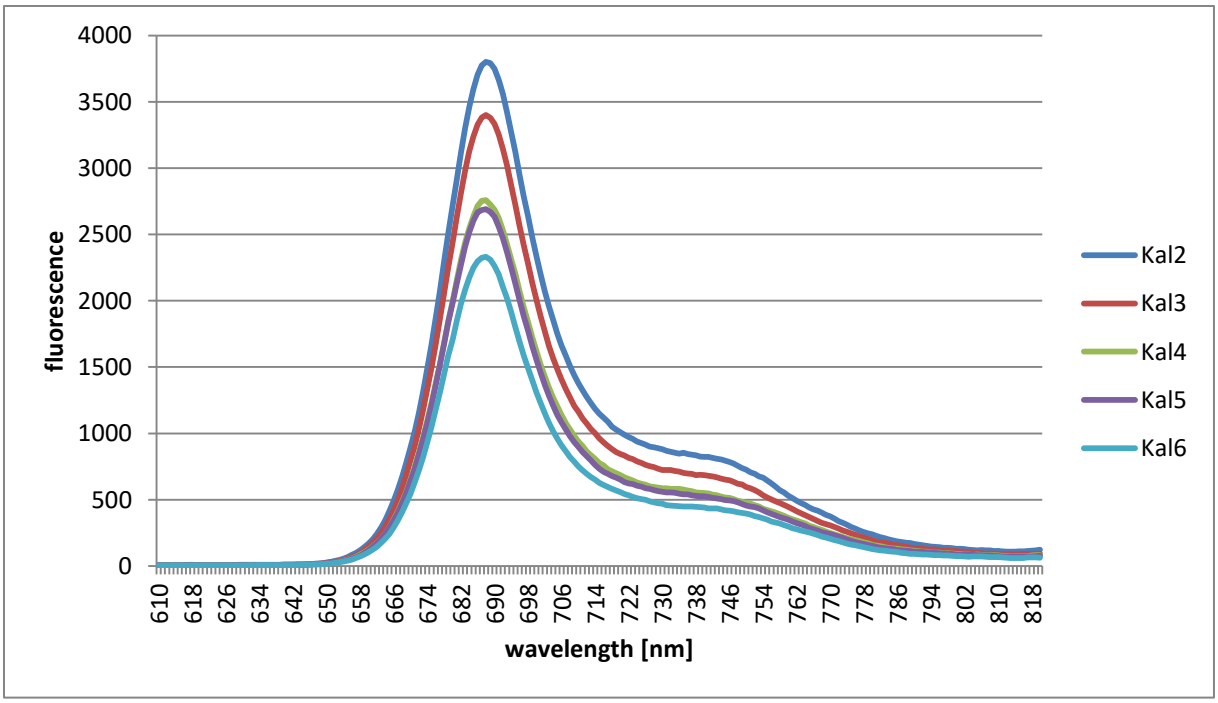

Illustration 41: Fluorescence spectra of the five algae concentrations of the green algae received by the Fluorimeter

As conclusion could be recorded that algae fluorescence and algae cell number have a linear correlation and are possible to detect and quantify by a simple and cheap routine on the microscope.

5.3. Oxygen gradient measurements with a Sensicam

The calibration of the sensicam method was undertaken with oxygen particles desolved in water. The upper chamber was filled with water including sodium sulfide, which replace free oxygen in the water. Therefore the upper chamber is colored by the program in red for the lack of oxygen and the lower chamber is blue what an indicator for oxygen presence is.

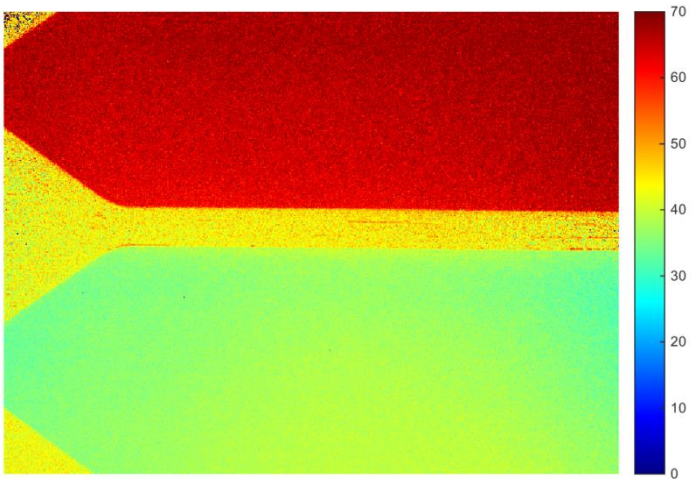

Illustration 42: calibration solutions for sensicam measurements, upper chamber filled with water including sodium sulfide and oxygen particles, lower chamber filled with water and oxygen particles

The reference measurements with chips filled with particles dispensed in pure Milli-Q water or media gave no differences on the sensicam results.

Also the measurements for algae and media without particles showed no difference in signal for which reason cross influences could be excluded. Only stray light could be seen in Illustration 43.

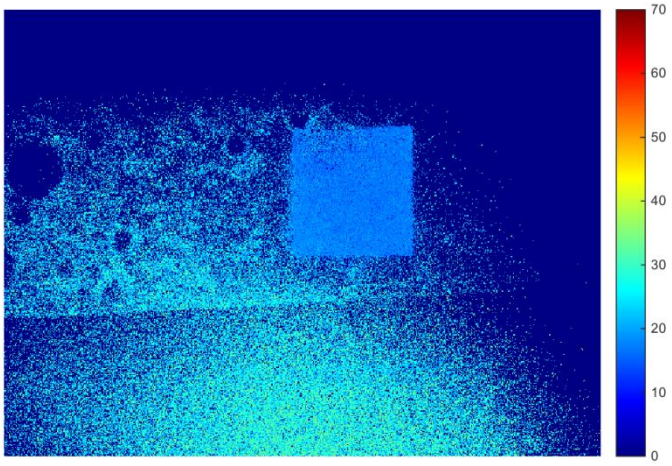

Illustration 43: algae without particles, only stray light could be seen

In cultivated 250 µl chips with green algae could be recognized a gradient if fresh media is pumped through the chip (with a flow 12.5 µl/min). This is the reason why most algae are grown at the inlet side of the chip.

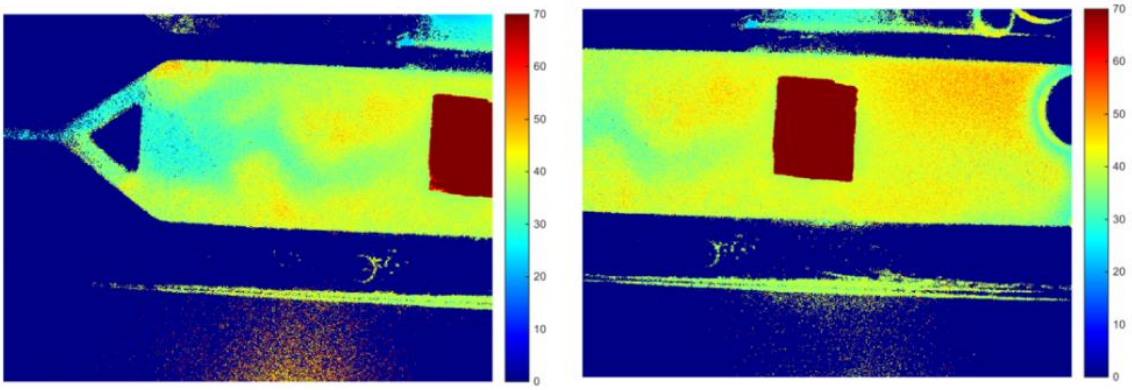

Illustration 44: Result-pictures for lifetime measurements with the sensicam

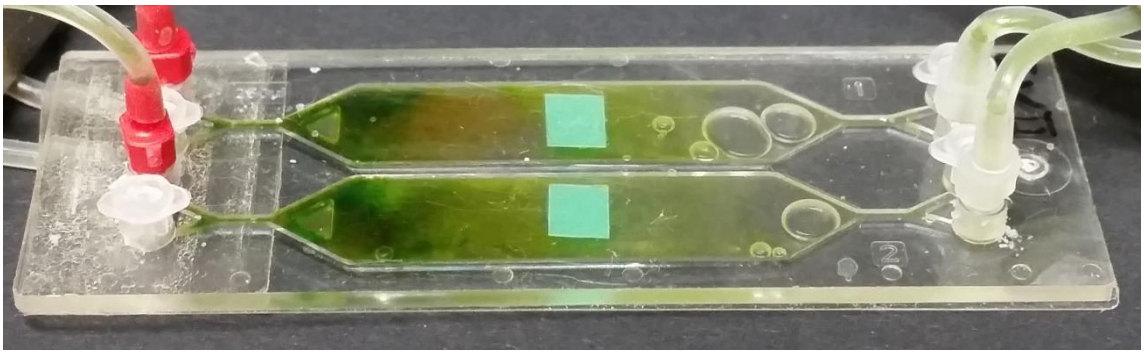

Illustration 45: Measured chip with green algae

All pictures in Illustration 46 show the same chamber filled with green algae. The first one represents the algae after addition of oxygen particles to the whole chamber and switching off the light. On the second one the algae had no light for 2 minutes, the third one was taken after 5 minutes, the fourth after 10 minutes, the fifth after 15 minutes and the last picture was made after 20 minutes. The algae started to consume the oxygen in the chamber after light and flow were switched off and a clear gradient could be observed where more algae were growing on the chip.

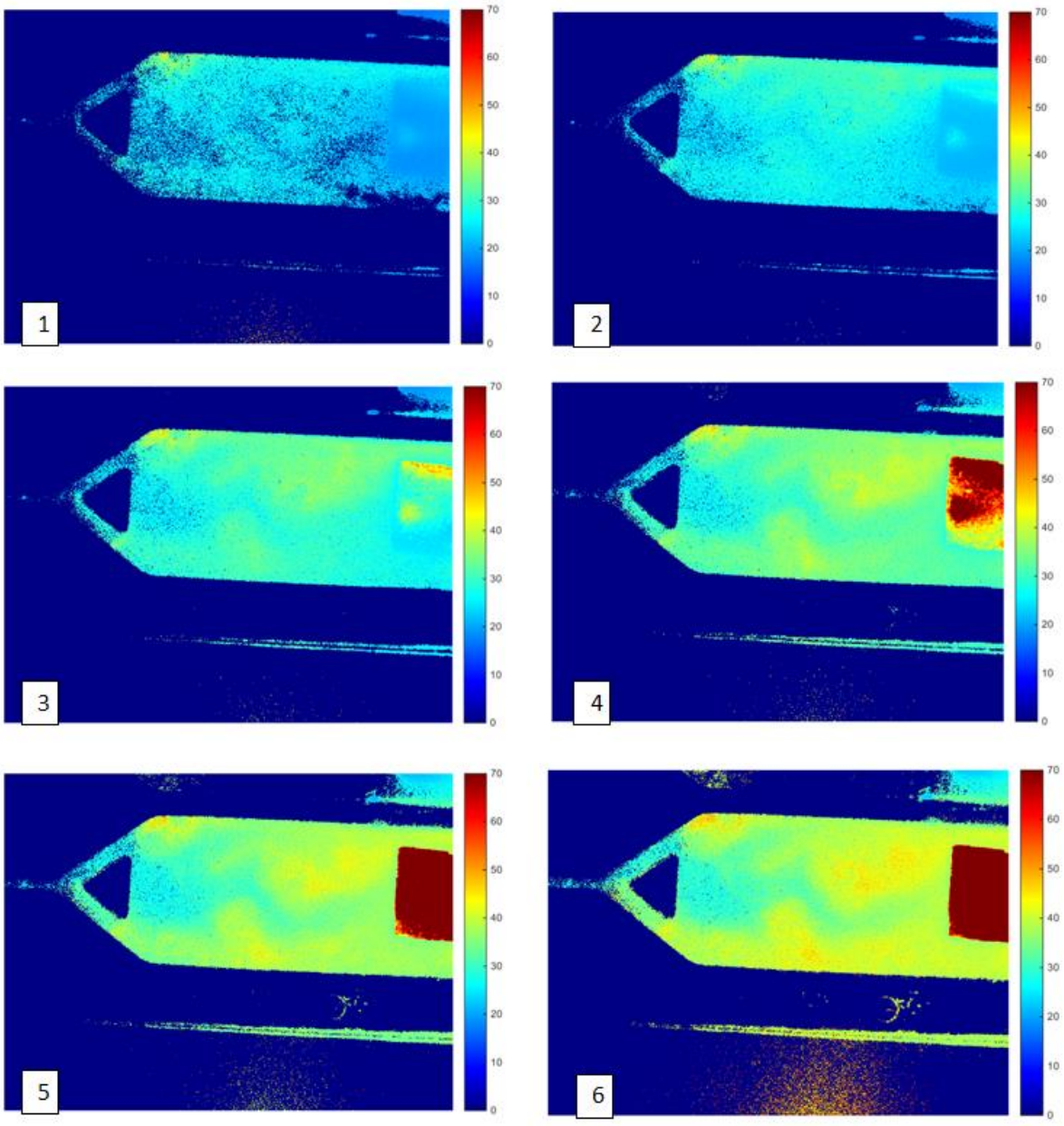

Illustration 46: Oxygen consumption by green algae over a period of 20 min in the dark

The examined 10 µl chips with green algae seeded 3 hours and 1 day with a flow of 1 µl/min and 5 min light and 5 min dark showed no good results because air bubbles came into chips and pushed the algae out.

The further experiments with 20 µl chips gave better results. A slight gradient could be seen between inlet and outlet.

Because of good handling with the 20 µl chips, for the reason that air bubbles can be pulled out, they were used for further experiments.

5.4. Relationship between the gradient of pO_2 and cell number

First experiments with the 10 µl chambers with three integrated oxygen sensor spots showed that there is a problem in evaluation of the data of the spots on outlet and inlet side. The middle spot gave most reliable data for further experiments and data evaluation.

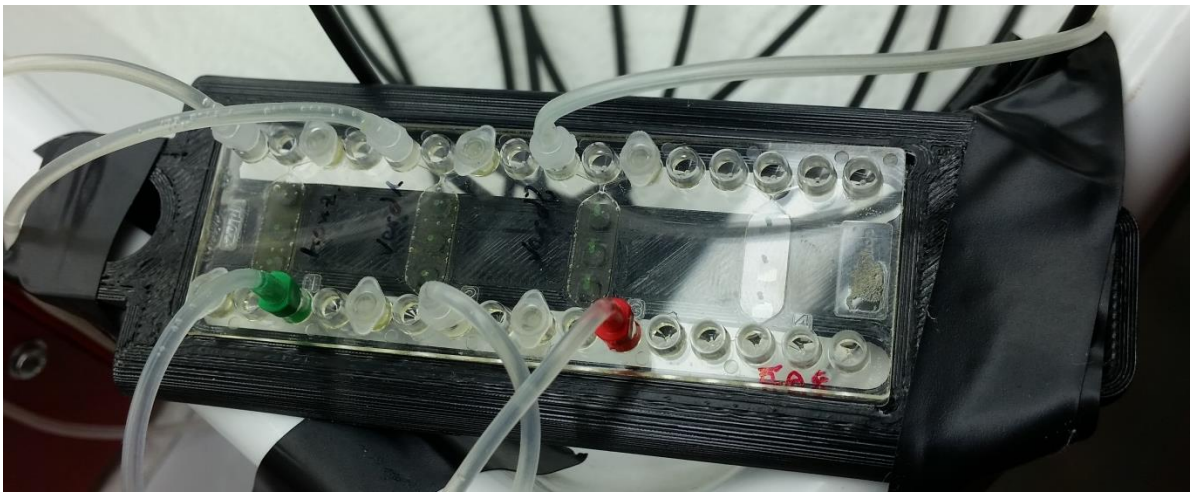

Illustration 47: used 10 µl rhombic chamber chip filled with three different concentrations of green algae

Also a reproducible measuring principle had to be determined.

Most of the experiments were done with green algae. Two measurements each were performed for gold algae and flint algae.

The gradient was obtained from the first 10 minutes of oxygen measurement data after switching off the light. Illustration 48 shows exemplary the oxygen measurement data of three different concentrations of green algae in the timescale of 10 minutes in the dark. Higher cell concentrations result in a steeper gradient of the oxygen measurement data.

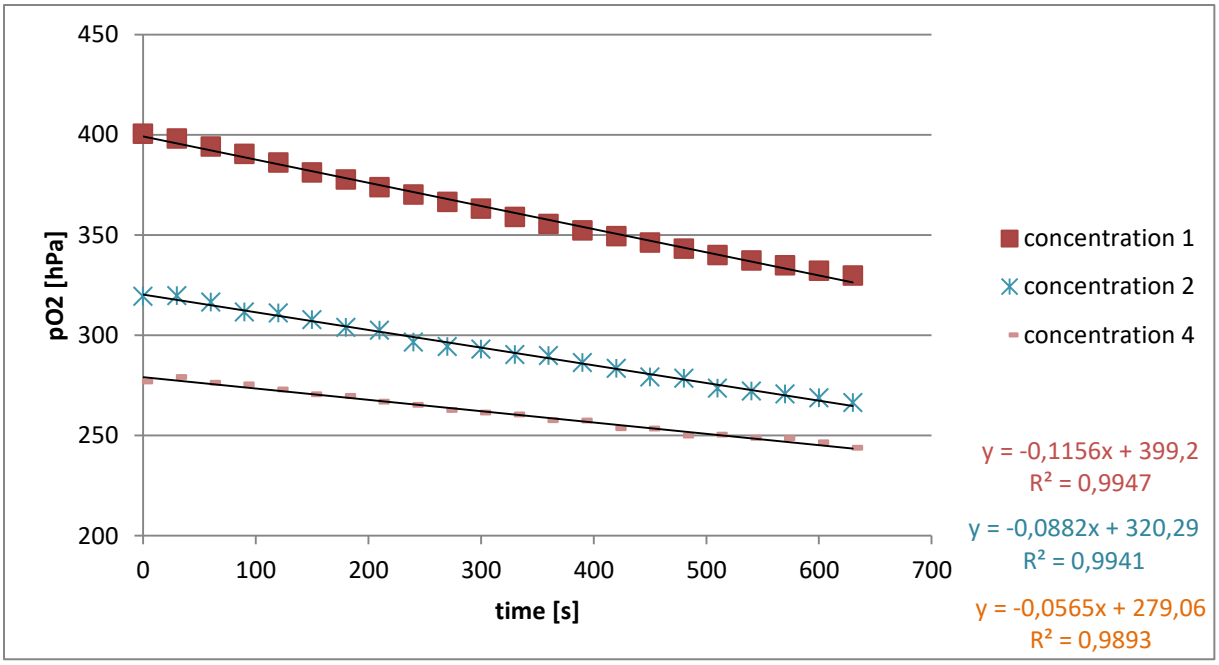

Illustration 48: oxygen measurement data of three different concentrations of green algae after the light was switched off

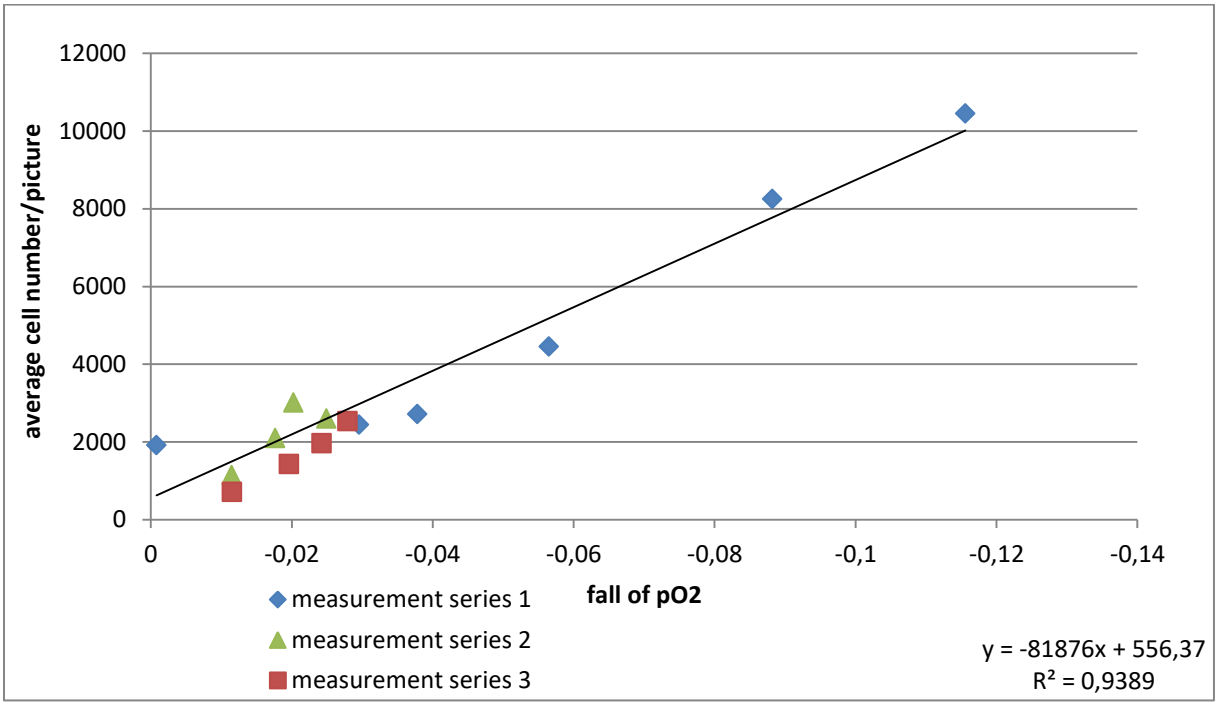

Illustration 49: Relationship between cell number and fall of pO_2 for the green algae (middle spot)

Measurements were taken on different days and at different concentrations, but the data fits together in a straight line. There is a correlation between cell number and oxygen fall for the green algae. The oxygen fall occurs immediately after light is switched off, due to the fact that algae consume oxygen during dark phase.

For the gold algae no statement for the conjunction between fall of pO_2 and cell number could be made, because of movements of the algae in the chip. This means that the microscope pictures could not be evaluated accurately.

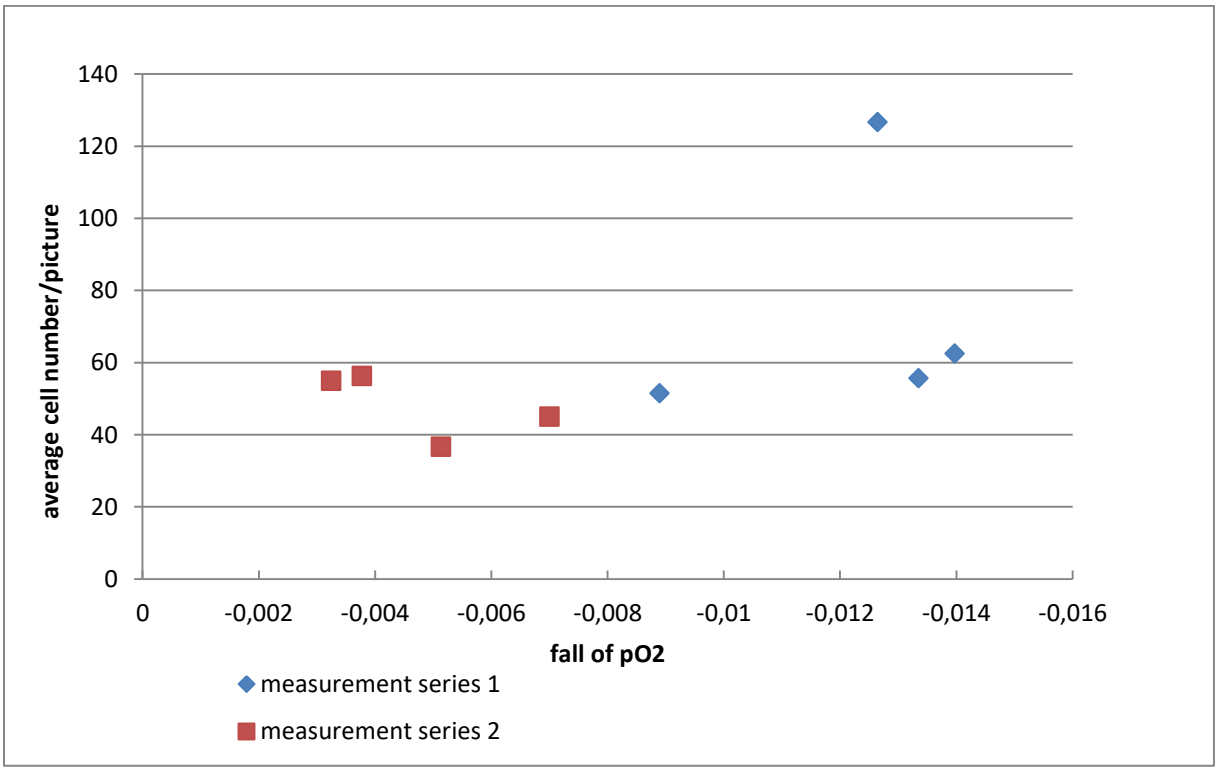

Illustration 50: Relationship between cell number and fall of pO_2 for the gold algae (no conjunction possible to obtain)

For the flint algae the conjunction worked, but due to the fact of the small size of the algae higher light exposition for the detection of pictures on the microscope was needed.

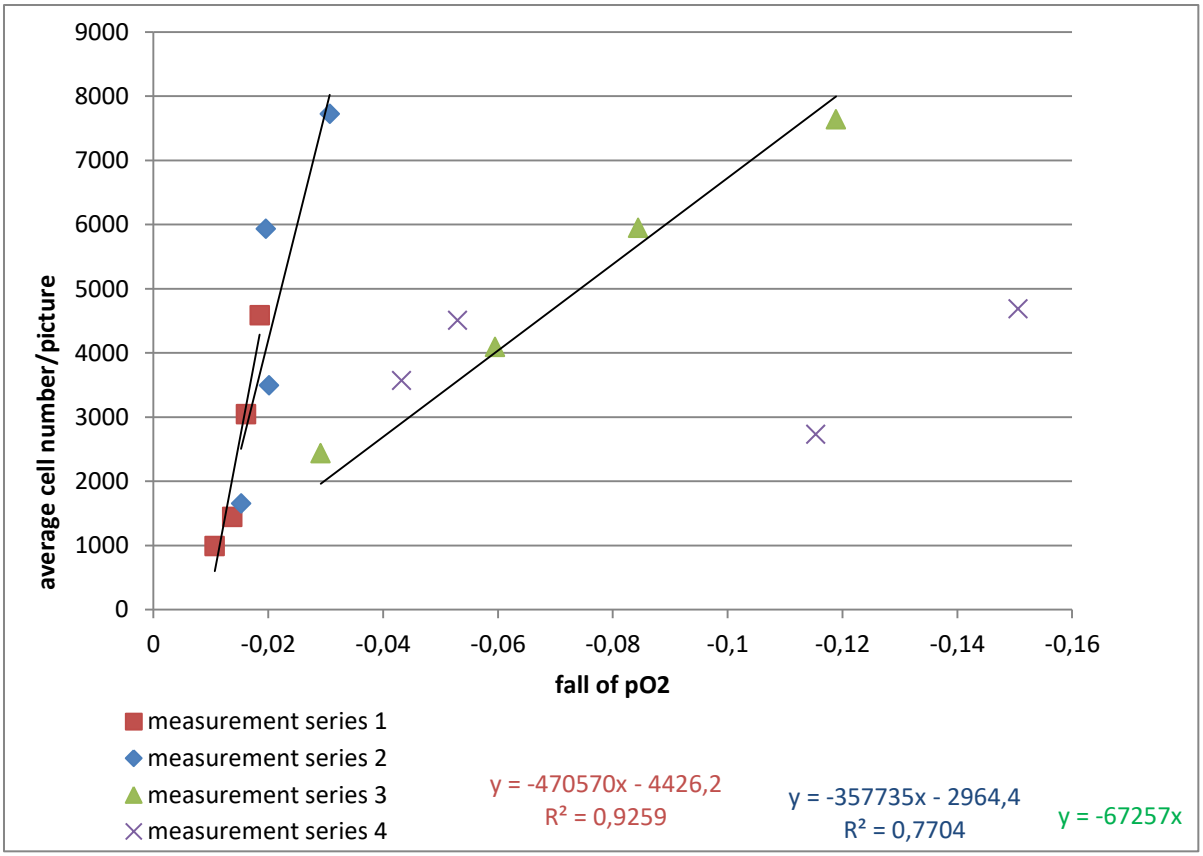

Illustration 51: Relationship between cell number and fall of pO_2 for the flint algae

6. Conclusion

Closing could be stated that the cultivation of algae in microfluidic chips was successfully transferred from the cultivation in batch cultures. Integration of oxygen sensor spots rendered possible monitoring of the course of oxygen values over whole days and nights with small optical detection devices.

The main results could be summarized as algae produce oxygen during light phase and consume it during dark phase. A correlation between fluorescence and algae cell number was obtained on the microscope. Furthermore an easy cell counting method was developed on the microscope including counting with the program ImageJ. Also a relationship between cell number and the gradient of oxygen during dark phase was received for green and flint algae. The gold algae were moving too fast to take an analyzable picture on the microscope.

Summarized best test procedure was obtained with chlorella vulgaris, a type of green algae, because of their size and low mobility. Concluding, a rapid respiration assay was successfully implemented.

7. Register of Illustrations

8. Register of Tables

References

[1] F. Baldini, A.N. Chester, J. Homola, S. Martellucci, ed., *Optical Chemical Sensors*, NATO Sciences Series, 2004.

[2] Y.L. P.R.Lang, ed., *Soft Matter at Aqueous Interfaces*, Springer, 2016.

[3] B. Valeur, *Molecular Fluorescence*, Wiley-VCH, Weinheim, 2002.

[4] X.-d. Wang and O. S. Wolfbeis, "Optical methods for sensing and imaging oxygen: Materials, spectroscopies and applications," *Chemical Society reviews*, vol. 43, no. 10, pp. 3666–3761, 2014.

[5] J. R. Lakowicz, *Principles of fluorescence spectroscopy*, Springer, New York, 2006.

[6] S. M. Borisov, G. Nuss, and I. Klimant, "Red light-excitable oxygen sensing materials based on platinum(II) and palladium(II) benzoporphyrins," *Analytical chemistry*, vol. 80, no. 24, pp. 9435–9442, 2008.

[7] A. H. G. Boisde, ed., *Chemical and biochemical sensing with optical fibres and waveguides*, Artech House, 1996.

[8] P. M. I.W. Donald, "Infrared transmitting materials," *J.Mat.Sci.*, pp. 1151–1176, 1978.

[9] S. Hocde, C. Pledel-Boussard, C. Fonteneau, G. J. Lucas, "TeAsSe glass fibers for evanescent wave spectroscopy," *Proc. SPIE,* no. 3849, 1999.

[10] R. Falciai, F. Baldini, F. Cosi, P. Bechi, F. Pucciani, "Bile enterogastric reflux sensor using plastic optical fibres," *Fiber and Integr. Opt.*, 1993.

[11] M.F. Vaezi, R.G. Lacamera, J.E. Richter, "Validation studies of Bilitec 2000: an ambulatory duodenogastrix reflux monitoring system," *Am.J.Physiol.*, 1994.

[12] "Seminar Microfluidics," http://mafija.fmf.uni-lj.si/seminar/files/2007_2008/Microfluidics-final.pdf.

[13] F. Lefèvre, A. Chalifour, L. Yu et al., "Algal fluorescence sensor integrated into a microfluidic chip for water pollutant detection," *Lab on a chip*, vol. 12, no. 4, pp. 787–793, 2012.

[14] "basic concepts of microfluidics," http://faculty.washington.edu/yagerp/microfluidicstutorial/basicconcepts/basiccon cepts.htm.

[15] G. Zheng, Y. Wang, Z. Wang et al., "An integrated microfluidic device in marine microalgae culture for toxicity screening application," *Marine pollution bulletin*, vol. 72, no. 1, pp. 231–243, 2013.

[16] S. Q. T.M. Squires, “Microfluidics: fluid physics at the nanolitre scale,” *Rev. Mod. Phys.,* no. 77, pp. 977–10216, 2005.

[17] D. P. D. Figeys, “Lab-on-a-chip: a revolution in biological and medical sciences,” *Analytical chemistry,* no. 72, 330 A-335 A, 2000.

[18] D.R. Reyes, D. Issoigidis, P.-A.Auroux, A. Manz, “Micro total analysis systems, 1. Introduction, theory and technology,” *Analytical chemistry,* no. 74, pp. 2623–2636, 2002.

[19] A. B. Peter Schopfer, ed., *Pflanzenphysiologie*, Springer, 2010.

[20] G. Eugene Rabinowitch, ed., *Photosynthesis*, John Wiley and Sons, Inc., 1969.

[21] J. Moroney, “Algal photosynthesis,” *Handbook of Plant Science*, vol. 2, pp. 1268–1273, 2007.

[22] Wilhelm Nultsch, ed., *Allgemeine Botanik*: *Kurzes Lehrbuch für Mediziner und Naturwissenschaftler*, Thieme, Stuttgart, 1977.

[23] P. J. D. Janssen, M. D. Lambreva, N. Plumeré et al., “Photosynthesis at the forefront of a sustainable life,” *Frontiers in chemistry*, vol. 2, p. 36, 2014.

[24] Carol Robinson, Peter J. le B. Williams, “Respiration and its measurement in surface marine waters: chapter 9,” 2004.

[25] M. Warkentin, H. M. Freese, U. Karsten et al., “New and fast method to quantify respiration rates of bacterial and plankton communities in freshwater ecosystems by using optical oxygen sensor spots,” *Applied and environmental microbiology*, vol. 73, no. 21, pp. 6722–6729, 2007.

[26] B. A. Wagner, S. Venkataraman, and G. R. Buettner, “The rate of oxygen utilization by cells,” *Free radical biology & medicine*, vol. 51, no. 3, pp. 700–712, 2011.

[27] B. KOK, “ON THE INTERRELATION OF RESPIRATION AND PHOTOSYNTHESIS IN GREEN PLANTS,” *BIOCHIMICA ET BIOPHYSICA ACTA*, vol. 1949, no. 3, pp. 625–631.

[28] E.A. Verde and L. R. McCloskey, “Photosynthesis and respiration of two species of algal symbionts in the anemone Anthopleura elegantissima (Brandt) (Cnidaria; Anthozoa),” *Journal of Experimental Marine Biology and Ecology*, vol. 195, no. 2, pp. 187–202, 1996.

[29] Xiaoping Xue, David A. Gauthier, David H. Turpin, Harold G. Weger, “Interactions between Photosynthesis and Respiration in the Green Alga Chlamydomonas reinhardti: Characterization of Light-Enhanced Dark Respiration,” *Plant Physiology*, vol. 1996, pp. 1005–1014.

[30] Haijiang Tai, Yuting Yang, Shuangyin Liu et al., “A Review of Measurement Methods of Dissolved Oxygen in Water.,”.

[31] S. Zieger, “Optical detection module for algae species used as early warning system,” 2015.